Cell

BET Bromodomain Inhibition as a Therapeutic Strategy to Target c-Myc

Jake E. Delmore,[1,9] Ghayas C. Issa,[1,9] Madeleine E. Lemieux,[2] Peter B. Rahl,[3] Junwei Shi,[4] Hannah M. Jacobs,[1] Efstathios Kastritis,[1] Timothy Gilpatrick,[1] Ronald M. Paranal,[1] Jun Qi,[1] Marta Chesi,[5] Anna C. Schinzel,[1] Michael R. McKeown,[1] Timothy P. Heffernan,[1] Christopher R. Vakoc,[4] P. Leif Bergsagel,[5] Irene M. Ghobrial,[1,6] Paul G. Richardson,[1,6] Richard A. Young,[3,7] William C. Hahn,[1,8] Kenneth C. Anderson,[1,6] Andrew L. Kung,[2] James E. Bradner,[1,6,*] and Constantine S. Mitsiades[1,6,*]

[1]Department of Medical Oncology, Dana-Farber Cancer Institute, 450 Brookline Avenue, Boston, MA 02215, USA
[2]Department of Pediatric Oncology, Dana-Farber Cancer Institute and Children's Hospital Boston, 450 Brookline Avenue, Boston, MA 02215, USA
[3]Whitehead Institute for Biomedical Research, 9 Cambridge Center, Cambridge, MA 02142, USA
[4]Cold Spring Harbor Laboratory, 1 Bungtown Road, Cold Spring Harbor, NY 11724, USA
[5]Comprehensive Cancer Center, Mayo Clinic Arizona, Scottsdale, AZ 85259, USA
[6]Department of Medicine, Harvard Medical School, 25 Shattuck Street, Boston, MA 02115, USA
[7]Department of Biology, Massachusetts Institute of Technology, Cambridge, MA 02142, USA
[8]Broad Institute of Harvard and MIT, 7 Cambridge Center, Cambridge, MA 02142, USA
[9]These authors contributed equally to this work
*Correspondence: james_bradner@dfci.harvard.edu (J.E.B.), constantine_mitsiades@dfci.harvard.edu (C.S.M.)
DOI 10.1016/j.cell.2011.08.017

SUMMARY

MYC contributes to the pathogenesis of a majority of human cancers, yet strategies to modulate the function of the c-Myc oncoprotein do not exist. Toward this objective, we have targeted *MYC* transcription by interfering with chromatin-dependent signal transduction to RNA polymerase, specifically by inhibiting the acetyl-lysine recognition domains (bromodomains) of putative coactivator proteins implicated in transcriptional initiation and elongation. Using a selective small-molecule bromodomain inhibitor, JQ1, we identify BET bromodomain proteins as regulatory factors for c-Myc. BET inhibition by JQ1 downregulates *MYC* transcription, followed by genome-wide downregulation of Myc-dependent target genes. In experimental models of multiple myeloma, a Myc-dependent hematologic malignancy, JQ1 produces a potent antiproliferative effect associated with cell-cycle arrest and cellular senescence. Efficacy of JQ1 in three murine models of multiple myeloma establishes the therapeutic rationale for BET bromodomain inhibition in this disease and other malignancies characterized by pathologic activation of c-Myc.

INTRODUCTION

c-Myc is a master regulatory factor of cell proliferation (Dang et al., 2009). In cancer, pathologic activation of c-Myc plays a central role in disease pathogenesis by the coordinated upregulation of a transcriptional program influencing cell division, metabolic adaptation, and survival (Dang, 2009; Kim et al., 2008). Amplification of *MYC* is among the most common genetic alterations observed in cancer genomes (Beroukhim et al., 2010). Validation of c-Myc as a therapeutic target is supported by numerous lines of experimental evidence. Murine models of diverse malignancies have been devised by introducing genetic constructs overexpressing *MYC* (Harris et al., 1988; Leder et al., 1986; Stewart et al., 1984). In addition, conditional transgenic models featuring tunable transcriptional suppression have shown that even transient inactivation of *MYC* is capable of promoting tumor regression (Jain et al., 2002; Soucek et al., 1998; Soucek et al., 2002). Elegant studies of systemic induction of a dominant-negative *MYC* allele within an aggressive, *KRAS*-dependent murine model of lung adenocarcinoma have further suggested the putative therapeutic benefit of c-Myc inhibition (Fukazawa et al., 2010). Importantly, these studies establish the feasibility of c-Myc inhibition within an acceptable therapeutic window of tolerability.

Nevertheless, a therapeutic approach to target c-Myc has remained elusive. The absence of a clear ligand-binding domain establishes a formidable obstacle toward direct inhibition, which is a challenging feature shared among many compelling transcriptional targets in cancer (Darnell, 2002). c-Myc functions as a DNA-binding transcriptional activator upon heterodimerization with another basic-helix-loop-helix leucine zipper (bHLH-LZ) transcription factor, Max (Amati et al., 1993; Blackwood and Eisenman, 1991). High-resolution structures of the complex fail to identify a hydrophobic involution compatible with the positioning of an organic small molecule (Nair and Burley, 2003).

Therefore, we have targeted c-Myc transcriptional function by another means, namely the disruption of chromatin-dependent signal transduction (Schreiber and Bernstein, 2002). c-Myc transcription is associated locally and globally with increases in histone lysine side-chain acetylation, a covalent modification of chromatin that is regionally associated with transcriptional

activation (Frank et al., 2003; Vervoorts et al., 2003). Histone acetylation templates the assembly of higher-ordered transcriptional complexes by recruiting proteins with one or more acetyl-lysine-binding modules or bromodomains (Dhalluin et al., 1999; Haynes et al., 1992). Members of the bromodomain and extraterminal (BET) subfamily of human bromodomain proteins (BRD2, BRD3, and BRD4) associate with acetylated chromatin and facilitate transcriptional activation by increasing the effective molarity of recruited transcriptional activators (Rahman et al., 2011). Notably, BRD4 has been shown to mark select M/G1 genes in mitotic chromatin as transcriptional memory and direct postmitotic transcription (Dey et al., 2009) via direct interaction with the positive transcription elongation factor complex b (P-TEFb) (Bisgrove et al., 2007). The discovery that c-Myc regulates promoter-proximal pause release of Pol II, also through the recruitment of P-TEFb (Rahl et al., 2010), established a rationale for targeting BET bromodomains to inhibit c-Myc-dependent transcription.

Recently, we reported the development and biochemical characterization of a potent, selective small-molecule inhibitor of BET bromodomains, JQ1 (Figure 1A) (Filippakopoulos et al., 2010). JQ1 is a thieno-triazolo-1,4-diazepine that displaces BET bromodomains from chromatin by competitively binding to the acetyl-lysine recognition pocket. In the present study, we leverage the properties of JQ1 as a chemical probe (Frye, 2010) to interrogate the role of BET bromodomains in Myc-dependent transcription and to explore the role of BET bromodomains as cancer dependencies.

Multiple myeloma (MM) represents an ideal model system for these mechanistic and translational questions, given the known role of *MYC* in disease pathophysiology. MM is an incurable hematologic malignancy that is typified by the accumulation of malignant plasma cells harboring diverse genetic lesions (Chapman et al., 2011). Dysregulation of transcription factors features prominently in the biology of MM, including NF-κB (Keats et al., 2007), c-Maf (Hurt et al., 2004), XBP1 (Claudio et al., 2002), HSF1 (Mitsiades et al., 2002), GR (Gomi et al., 1990), IRF4 (Shaffer et al., 2008), Myb (Palumbo et al., 1989), and, notably, c-Myc (Dean et al., 1983). Rearrangement or translocation of *MYC* are among the most common somatic events in early- and late-stage MM (Shou et al., 2000), and transcriptional profiling identifies Myc pathway activation in more than 60% of patient-derived MM cells (Chng et al., 2011). Experimental support for the central role of c-Myc in the pathogenesis of MM is contributed by an informative, genetically engineered murine model of MM. Lineage-specific and stochastic activation-induced deaminase (AID)-dependent activation of a conditional *MYC* transgene in the late stages of B cell differentiation establishes genetically engineered mice with a plasma cell malignancy that shares clinically relevant features of MM (Chesi et al., 2008). Thus, *MYC* dysregulation represents a largely unifying molecular feature observed across the otherwise complex genetic landscape of MM.

In this study, we report that c-Myc transcriptional function can be modulated pharmacologically by BET bromodomain inhibition. Unexpectedly, we have discovered that *MYC* itself is transcriptionally regulated by BET bromodomains. Chromatin immunoprecipitation studies show that BRD4 is strongly enriched at immunoglobulin heavy-chain (IgH) enhancers in MM cells bearing IgH rearrangement at the *MYC* locus. BET inhibition with JQ1 depletes enhancer-bound BRD4 and promptly inhibits *MYC* transcription in a dose- and time-dependent manner. In translational models of MM, JQ1 leads to depletion of the c-Myc oncoprotein and selective downregulation of the coordinated c-Myc transcriptional program, prompting cell-cycle arrest and cellular senescence. These results indicate that targeting protein-protein interactions within the c-Myc transcriptional signaling network can modulate the function of c-Myc in cancer.

RESULTS

BET Bromodomains as Therapeutic Targets in MM

We first evaluated the expression of *BRD2*, *BRD3*, *BRD4*, and *BRDT* transcripts in MM by integrating publicly available compendia of gene expression data sets. Among asymptomatic patients with premalignant disease (Zhan et al., 2007), we observed increasing expression of *BRD4* in monoclonal gammopathy of undetermined significance (MGUS) and smoldering MM (SMM) compared to normal bone marrow plasma cells (Figure 1B). In a second, independent data set (Mattioli et al., 2005), we observed significantly higher expression of *BRD4* in plasma cell leukemia (PCL) compared to MM or MGUS samples (Figure 1C). Thus, *BRD4* expression correlates positively with disease progression. *BRD2* and *BRD3* are also expressed in MM, but expression does not clearly correlate with stage of disease (data not shown). *BRDT*, a testis-specific bromodomain-containing protein, is not expressed in MM.

Analysis of copy number polymorphism (CNP) data collected on 254 MM patients by the Multiple Myeloma Research Consortium (MMRC) revealed that the *BRD4* locus is frequently amplified in MM patient samples (Figure 1D). The majority of patient samples exhibit broad amplification of chromosome 19p, but focal amplification at the *BRD4* locus is observed (Figure S1 available online). Among 45 established MM cell lines, expression of BRD4 was pronounced and did not correlate with amplification status (Figure 1E).

Human MM cells are highly osteotropic in vivo, and interaction with bone marrow stromal cells (BMSCs) induces proliferation and contributes to drug resistance (McMillin et al., 2010). Analysis of BET bromodomain expression, as influenced by MM cell binding to BMSCs (McMillin et al., 2010), revealed marked upregulation of BRD4 in the INA-6 human MM cell line upon interaction with HS5 stromal cells (Figure 1F), suggesting a plausible role for BRD4 function in MM cells within the bone marrow microenvironment.

To explore the function of BET bromodomains in MM, we examined the effect on proliferation of small hairpin RNAs (shRNAs) targeting each of the four BET proteins in comparison to shRNAs targeting 1011 kinases, phosphatases, and oncogenes in a lentivirally delivered, arrayed shRNA screen in INA-6 cells. As illustrated in Figures 1G and 1H, shRNA constructs targeting each of the expressed BET bromodomains are identified as reducing INA-6 proliferation as shown by normalized B scores (Malo et al., 2006). Together, these data establish

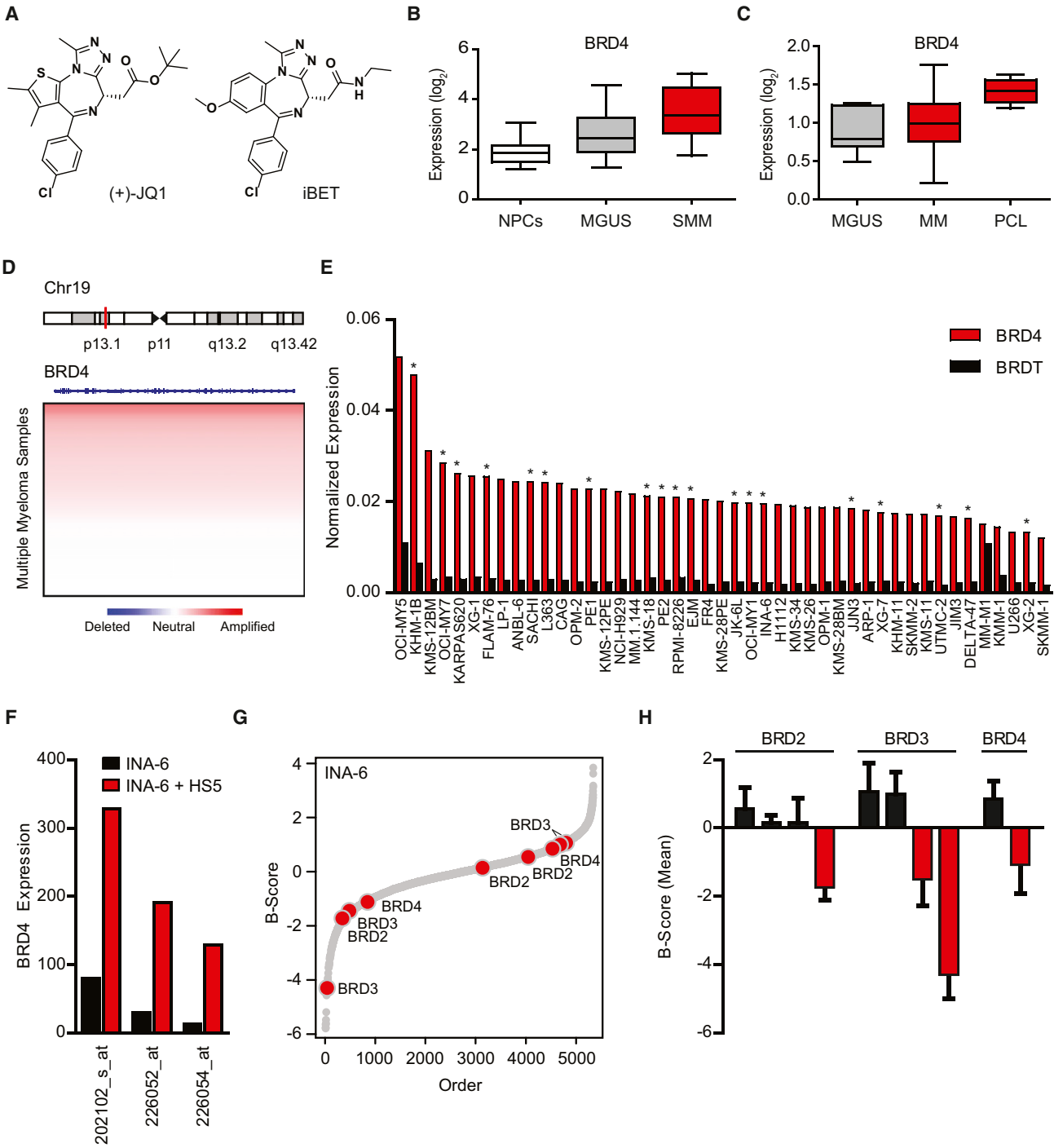

Figure 1. Integrated Genomic Rationale for BET Bromodomains as Therapeutic Targets in MM

(A) Structures of the BET bromodomain inhibitors JQ1 and iBET.

(B and C) Expression levels (log2 transformed, median-centered values) for *BRD4* transcripts were evaluated in oligonucleotide microarray data from normal plasma cells (NPCs) from healthy donors, individuals with MGUS, or SMM patients (B, data set GSE5900; Zhan et al., 2007) and in plasma cells from MGUS, MM, and PCL patients (C, data set GSE2113; Mattioli et al., 2005). Increased *BRD4* expression is observed in SMM (or MGUS) compared to NPCs (B) and in PCL compared to MM (C) (nonparametric Kruskal-Wallis one-way analysis of variance; $p < 0.001$ and $p = 0.0123$, respectively; Dunn's Multiple Comparison post-hoc tests; $p < 0.05$ in both cases). For each box plot, the whiskers represent minimum and maximum values, the lower and upper boundaries denote the 25th and 75th percentile, respectively, and the horizontal line represents the median value for each group.

(D) Copy number analysis of the *BRD4* locus at human chromosome 19p13.1 in primary samples from 254 MM patients. Chromosome 19p amplifications are common in MM. See also Figure S1.

a rationale for the study of BET bromodomains, and BRD4 in particular, as tumor dependencies in MM.

BET Inhibition with JQ1 Arrests c-Myc Transcriptional Programs

To test the hypothesis that BET inhibition will specifically abrogate Myc-dependent transcription, we utilized global transcriptional profiling and unbiased gene set enrichment analysis (GSEA). We first characterized the transcriptional consequences of BET inhibition in three MM cell lines with genetically distinct activating lesions at the *MYC* locus (KMS11, MM.1S, and OPM1) (Dib et al., 2008). Unsupervised hierarchical clustering segregated samples based on treatment assignment, suggesting a common transcriptional consequence in response to JQ1 (Figure 2A). Acute JQ1 treatment did not prompt global, nonspecific transcriptional silencing but instead produced significant changes in a finite number of genes (88 down- and 25 upregulated genes by 2-fold or greater in all three MM lines).

To examine higher-order influences on biological networks regulated by c-Myc, we evaluated four canonical transcriptional signatures of *MYC*-dependent genes (Kim et al., 2006; Schlosser et al., 2005; Schuhmacher et al., 2001; Zeller et al., 2003). All four signatures were strongly correlated with downregulation of expression by JQ1 (Figure 2B). As a measure of the specificity of this effect, an open-ended enrichment analysis was performed on the entire set of transcription factor target gene signatures available from the Molecular Signatures Database (MSigDB). Gene sets defined by adjacency to Myc-binding motifs were in almost all cases significantly enriched in JQ1-suppressed genes (Figures 2C and 2D). In marked contrast, JQ1 treatment did not exert significant suppression of gene sets for other transcription factors linked to pathophysiology of MM, including NF-κB, AP-1, STAT3, GR, and XBP-1 (Figure 2E and Figure S2). Notably, 27 of the 28 significantly correlated gene sets are annotated as predicted targets of MYC or E2F (Figure 2C and Figure S2). Consistent with Myc-specific inhibition, biological modules associated with Myc (e.g., ribosomal biogenesis and assembly and glycolysis) were also anticorrelated with JQ1 treatment (Figure 2E). BET bromodomain inhibition by JQ1 confers a selective repression of transcriptional networks induced by c-Myc.

Regulation of *MYC* Transcription by BET Bromodomains

An unexpected finding was the observed, robust inhibition of *MYC* expression following treatment with JQ1 (Figure 2A). As *MYC* is commonly activated by upstream oncogenic signaling pathways, we studied the consequence of JQ1 treatment on the expression of 230 cancer-related genes in a human MM cell line (MM.1S) using a multiplexed transcript detection assay (Figure 3A). Excellent concordance was observed between replicate measurements of expressed genes (Figure S3A). Unsupervised hierarchical clustering segregated replicate data correctly into early- and late-treatment time points. Surprisingly, we observed immediate, progressive, and profound downregulation of *MYC* transcription itself, a unique finding among all transcripts studied ($p < 0.05$).

Downregulation of *MYC* was further confirmed by RT-PCR and immunoblot (Figures 3B and 3C). This effect was BET bromodomain specific, supported by the nearly comparable activity of an analogous BET inhibitor subsequently published by Glaxo SmithKline (iBET) (Figure 1A) (Nicodeme et al., 2010) and the lack of activity of the inactive (-)- JQ1 enantiomer, which we previously characterized as structurally incapable of inhibiting BET bromodomains (Filippakopoulos et al., 2010) (Figure 3C). Inhibition of *MYC* transcription by JQ1 was observed to be dose and time dependent, with peak inhibition at submicromolar concentrations (Figures 3D and 3E). Rapid depletion of chromatin-bound c-Myc was confirmed by nuclear ELISA transcription factor-binding assays (Figure 3F). In contrast, NF-κB and AP-1 chromatin-binding assays failed to reveal any decrease in DNA binding within 8 hr of JQ1 treatment (Figure 3G and Figure S4A).

To assess the breadth of these findings in MM, we expanded gene expression studies to three MM cells with distinct lesions at the *MYC* locus. MM.1S cells have a complex *MYC* rearrangement involving an IgH insertion at the breakpoint of a derivative chromosome der3t(3;8); KMS-11 cells have both *MYC* duplication and inversion; and OPM1 cells feature a der(8)t(1;8) (Dib et al., 2008). Among 230 genes studied, *MYC* was one of only four genes downregulated by treatment with JQ1, along with *MYB*, *TYRO3*, and *TERT* (Figure 3H and Figure S4B). Immunoblotting analyses confirmed the JQ1 suppression of c-Myc protein expression in a further expanded panel of Myc-dependent MM cell lines (Figure 3I). Despite the intriguing potential effect on E2F transcriptional function and *MYB* gene expression, JQ1 did not influence E2F or MYB protein abundance through 24 hr of drug exposure (Figures S4C and S4D). Together, these data support the general observation that BET inhibition specifically suppresses *MYC* transcription across MM cells with different genetic lesions affecting the *MYC* locus and with striking selectivity in comparison to other oncogenic transcriptions factors with established roles in MM pathophysiology.

BRD4 Binds IgH Enhancers, Regulating *MYC* Expression and Function

Based on the integrated, functional genomic analysis of BET bromodomains in MM (Figure 1), we pursued further mechanistic studies of BRD4. Silencing of *BRD4* using directed shRNAs

(E) Expression levels of *BRD4* (compared to *BRDT*) in human MM cell lines. Asterisks denote cell lines with amplification of the *BRD4* locus (19p13.1).
(F) *BRD4* expression (depicted on a linear scale for three different oligonucleotide microarray probes) in INA-6 MM cells cultured in vitro in the presence or absence of HS-5 bone marrow stromal cells.
(G) Silencing of BET bromodomains impairs proliferation in MM cells. Results of an arrayed lentiviral screen using a diverse shRNA library in INA-6 MM cells are presented in rank order of ascending B scores. The effect of shRNAs targeting BET bromodomains on INA-6 cell viability is highlighted by red circles and annotated by gene. Gray dots represent results for non-BET bromodomain shRNAs.
(H) Silencing of BET bromodomain family members in MM cells. Viability of INA-6 MM cells exposed to shRNAs directed against BRD2, BRD3, and BRD4 are reported as mean B scores (± SD of the two normalized replicates).

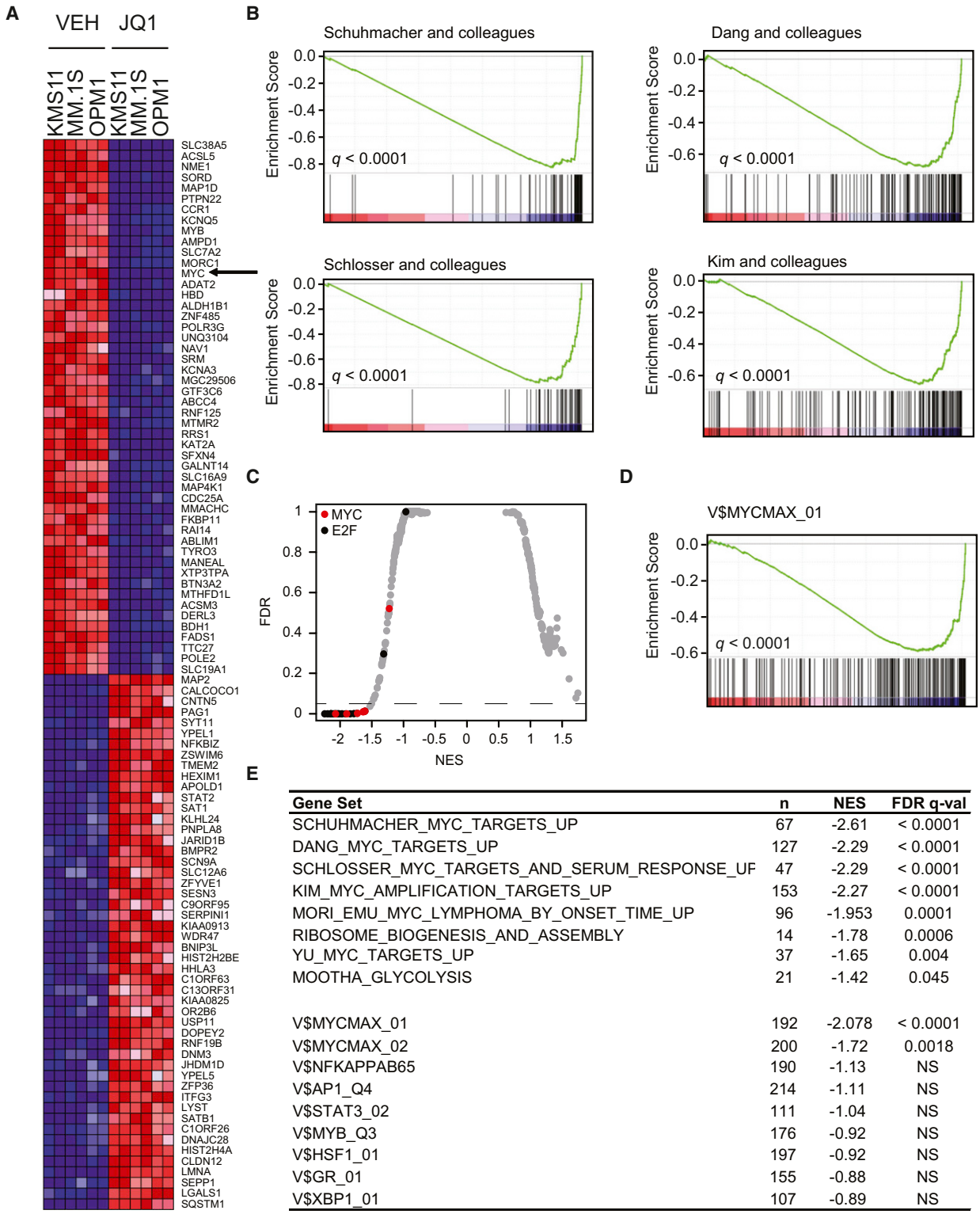

E

Gene Set	n	NES	FDR q-val
SCHUHMACHER_MYC_TARGETS_UP	67	-2.61	< 0.0001
DANG_MYC_TARGETS_UP	127	-2.29	< 0.0001
SCHLOSSER_MYC_TARGETS_AND_SERUM_RESPONSE_UP	47	-2.29	< 0.0001
KIM_MYC_AMPLIFICATION_TARGETS_UP	153	-2.27	< 0.0001
MORI_EMU_MYC_LYMPHOMA_BY_ONSET_TIME_UP	96	-1.953	0.0001
RIBOSOME_BIOGENESIS_AND_ASSEMBLY	14	-1.78	0.0006
YU_MYC_TARGETS_UP	37	-1.65	0.004
MOOTHA_GLYCOLYSIS	21	-1.42	0.045
V$MYCMAX_01	192	-2.078	< 0.0001
V$MYCMAX_02	200	-1.72	0.0018
V$NFKAPPAB65	190	-1.13	NS
V$AP1_Q4	214	-1.11	NS
V$STAT3_02	111	-1.04	NS
V$MYB_Q3	176	-0.92	NS
V$HSF1_01	197	-0.92	NS
V$GR_01	155	-0.88	NS
V$XBP1_01	107	-0.89	NS

Figure 2. Inhibition of Myc-Dependent Transcription by the JQ1 BET Bromodomain Inhibitor

(A) Heatmap representation of the top 50 down- and upregulated genes ($p < 0.001$) following JQ1 treatment in MM cell lines. Data are presented row normalized (range from −3- to 3 standard deviations from median in expression). *MYC* (arrow) is downregulated by JQ1 treatment.

(B) GSEA of four Myc-dependent gene sets (Kim et al., 2006; Schlosser et al., 2005; Schuhmacher et al., 2001; Zeller et al., 2003) in transcriptional profiles of MM cells treated (left) or untreated (right) with JQ1.

validated by RT-PCR analysis (Figure 4A) elicited a marked decrease in *MYC* transcription (Figure 4B) accompanied by G1 cell-cycle arrest in JQ1-sensitive MM cells (OPM-1) (Figure 4B and Figure S5A). We reasoned that early and sustained JQ1-induced suppression of *MYC* transcription may be mechanistically explained by physical interaction of BRD4 with regulatory elements influencing *MYC* expression. Indeed, avid binding of BRD4 to established IgH enhancers was observed by chromatin immunoprecipitation (ChIP) in MM.1S cells (Figure 4C and Figure S6), which harbor an IgH insertion proximal to the *MYC* transcriptional start site (TSS). BRD4 binding was not observed at five characterized enhancer regions adjacent to the *MYC* gene (Pomerantz et al., 2009a, 2009b). JQ1 treatment (500 nM) for 24 hr significantly depleted BRD4 binding to IgH enhancers and the TSS, supporting direct regulation of *MYC* transcription by BET bromodomains and a model whereby BRD4 acts as a coactivator of *MYC* transcription potentially through long-range interactions with distal enhancer elements. Forced overexpression of c-Myc in MM cells (OPM1) by retroviral infection rescues, in part, the cell-cycle arrest observed with JQ1 treatment (Figures 4D and 4E), arguing that *MYC* downregulation by JQ1 contributes functionally to cell physiology in MM.

Therapeutic Implications of BET Inhibition in MM

Based on this mechanistic rationale, we evaluated the therapeutic opportunity of *MYC* transcriptional inhibition using established translational models of MM. Antiproliferative activity of JQ1 was assessed using a panel of 25 MM cell lines or isogenic derivative lines (Figure 5A). MM cell proliferation was uniformly inhibited by JQ1 (Figure 5A), including several MM cell lines selected for resistance to FDA-approved agents (dexamethasone-resistant MM.1R and melaphalan-resistant LR5). As expected, MM cells possessing diverse genetic lesions involving *MYC* (Dib et al., 2008) were comparably sensitive to JQ1 (Figure 5B).

As interaction of MM cells with BMSCs is widely recognized to confer resistance to numerous therapeutic agents (Hideshima et al., 2007; McMillin et al., 2010), we sought to characterize the effect of BMSCs on MM cell sensitivity to BET inhibition. Using compartment-specific bioluminescence imaging assays (CS-BLI), we observed that the sensitivity of MM cell lines to JQ1 is largely unchanged by the presence of HS-5 bone marrow stroma cells (Figure 5C). This pattern of broad activity in MM without evident stroma-mediated chemoresistance has been associated with efficacy of FDA-approved agents bortezomib and lenalidomide.

MM cells were then further phenotyped for Myc-specific biological effects of BET inhibition. Flow cytometry of JQ1-treated MM.1S cells revealed a pronounced decrease in the proportion of cells in S phase, with a concomitant increase in cells arrested in G0/G1 (Figure 6A). Only a modest induction of apoptosis was observed after 48 hr of JQ1 treatment (Figure 6B), in contrast to the nonselective cytotoxic kinase inhibitor staurosporine (Figure S5B). Transcripts previously associated with induction of cellular senescence were enriched following treatment with JQ1, by GSEA (Figure 6C). Experimentally, treatment with JQ1 resulted in pronounced cellular senescence by β-galactosidase staining (Figure 6D). Overall, these phenotypes of arrested proliferation, G1 cell-cycle arrest, and cellular senescence are highly specific to anticipated effects of inhibiting cellular c-Myc function (Wu et al., 2007).

We next extended the study of JQ1 in MM cells to primary MM samples. JQ1 exposure led to a significant reduction in cell viability among the majority of CD138+ patient-derived MM samples tested (Figure 7A). In primary cells isolated from a patient with relapsed/refractory MM, JQ1 treatment ex vivo conferred a time-dependent suppression of c-Myc expression (Figure 7B). In contrast, JQ1 treatment of phytohemaglutinin (PHA)-stimulated peripheral blood mononuclear cells (PBMCs) suppressed PHA-induced proliferation but did not adversely influence cell viability, indicating that the anti-MM effect of JQ1 is not accompanied by a nonspecific, toxic effect on all hematopoietic cells (Figure S7A).

To model the therapeutic effect of JQ1 in vivo, we evaluated anti-MM efficacy in multiple orthotopic models of advanced disease. First, JQ1 was studied using an established, bioluminescent MM model (MM.1S-luc), which recapitulates the clinical sequelae, anatomic distribution of MM lesions, and hallmark bone pathophysiology observed in MM patients (Mitsiades et al., 2004). Tumor-bearing mice were treated with JQ1 administered by intraperitoneal injection (50 mg/kg daily) or vehicle control. JQ1 treatment significantly decreased the burden of disease measured by serial, whole-body, noninvasive bioluminescence imaging (Figures 7C and 7D). Importantly, treatment with JQ1 resulted in a significant prolongation in overall survival compared to vehicle-treated animals (Figure 7E). In a second plasmacytoma xenograft that more accurately models extramedullary disease, JQ1 also exhibited a significant disease-modifying response (Figure S7B). Finally, the effect of JQ1 was explored in the genetically engineered model of MYC-dependent MM (Chesi et al., 2008). To date, two Vk*MYC mice with established disease and measurable M-protein have completed 14 days of JQ1 treatment (25 mg/kg daily, adjusted to tolerability). Both animals reveal objective evidence of response assessed by reduction of serum immunoglobulins, including a complete response (CR) in the second animal (Figure 7F and Figure S7C). In this faithful orthotopic and nonproliferative model, the only FDA-approved agents, bortezomib, melphalan and cyclophosphamide, have previously prompted a CR (Chesi et al., 2008). These results establish in vivo proof of concept

(C) Quantitative comparison of all transcription factor target gene sets available from the MSigDB by GSEA for reduced expression in JQ1-treated MM cell lines. Data are presented as scatterplot of false discovery rate (FDR) versus normalized enrichment score (NES) for each evaluated gene set. Colored dots indicate gene sets for MYC (red), E2F (black), or other (gray) transcription factors.

(D) GSEA showing downregulation in JQ1-treated MM cells of a representative set of genes with proximal promoter regions containing Myc-Max-binding sites.

(E) Table of gene sets enriched among genes downregulated by JQ1 in MM cells (top group), highlighting the number of genes in each set (n), the normalized enrichment score (NES), and test of statistical significance (FDR q value). The bottom group represents comparisons of top-ranking transcription factor target gene sets of MM master regulatory proteins, enriched among genes downregulated by JQ1 in MM cells. See also Figure S2.

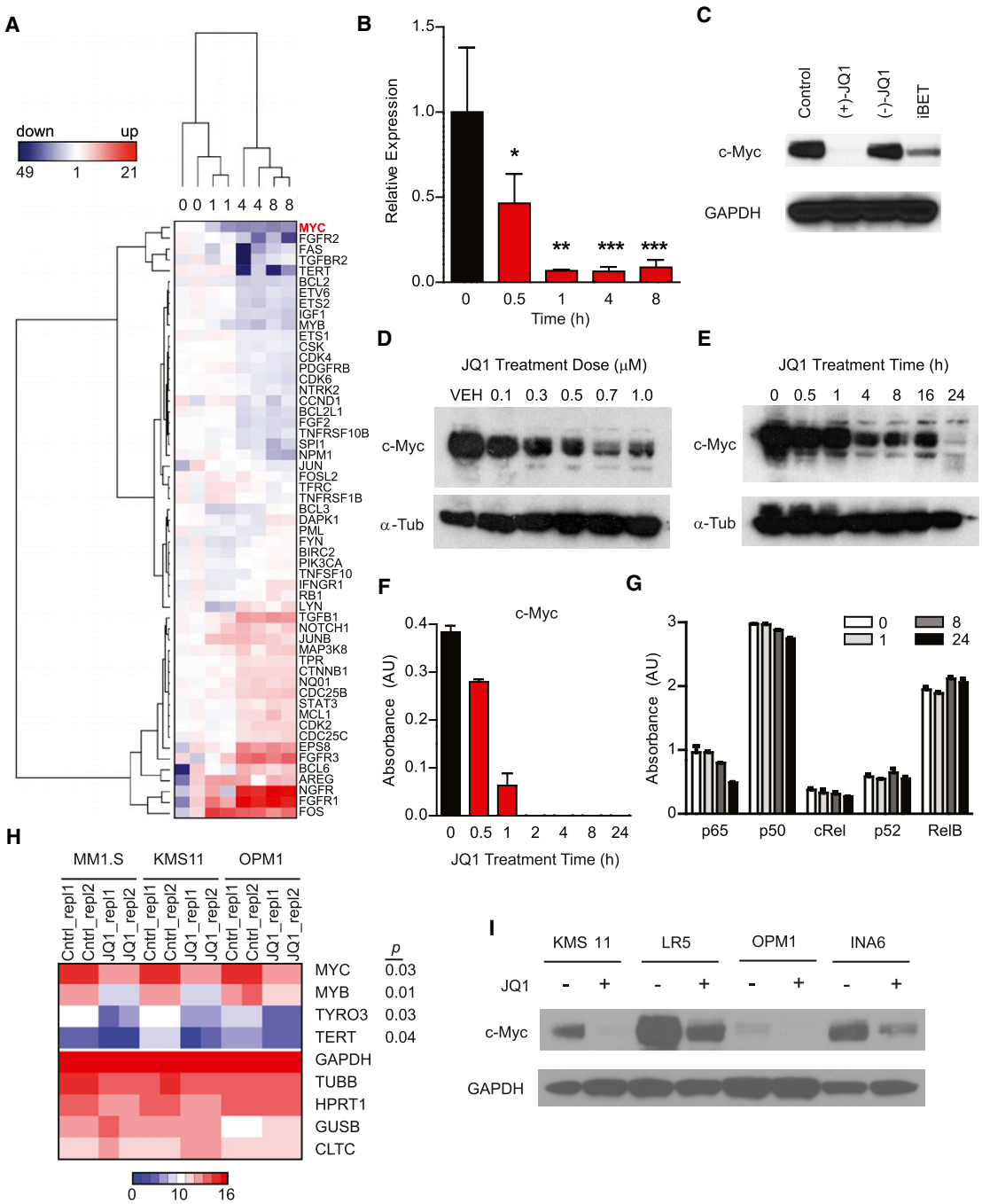

Figure 3. BET Inhibition Suppresses *MYC* Transcription in MM

(A) Heatmap of cancer-related genes expressed in MM cells (MM.1S), treated with JQ1 (500 nM over 1, 4, and 8 hr). *MYC* (red) is downregulated by JQ1 in a time-dependent manner, uniquely among all oncogenes studied (230 total). MYC was identified as the only statistically significant decrease in transcription at all four time points analyzed ($p < 0.05$). See also Figure S3.

(B) Quantitative RT-PCR analysis for *MYC* levels in JQ1-treated MM.1S cells (500 nM, 0–8 hr). Data are presented as ratio of *MYC* expression at each time point compared to baseline *MYC* expression (mean ± SD). Asterisks denote the level of statistical significance (*$p < 0.01$, **$p < 0.0002$, ***$p < 0.006$; paired Student's t test each relative to t = 0 hr).

(C) The active JQ1 enantiomer and the structurally analogous BET inhibitor iBET (Nicodeme et al., 2010), but not the inactive (-)-JQ1 enantiomer, downregulate c-Myc expression, as determined by immunoblotting of MM.1S cells treated with compounds (500 nM) or vehicle control for 24 hr.

(D and E) Immunoblotting analyses of the (D) dose- and (E) time-dependent effects of JQ1 treatment on c-Myc expression in MM.1S cells.

(F and G) Selective depletion of nuclear c-Myc following JQ1 treatment (500 nM) as measured by ELISA-based DNA-binding assays for the activity of (F) c-Myc (depleted after 1–2 hr) and (G) NF-κB family members (unaffected). Data represent mean ± SEM. See also Figure S4.

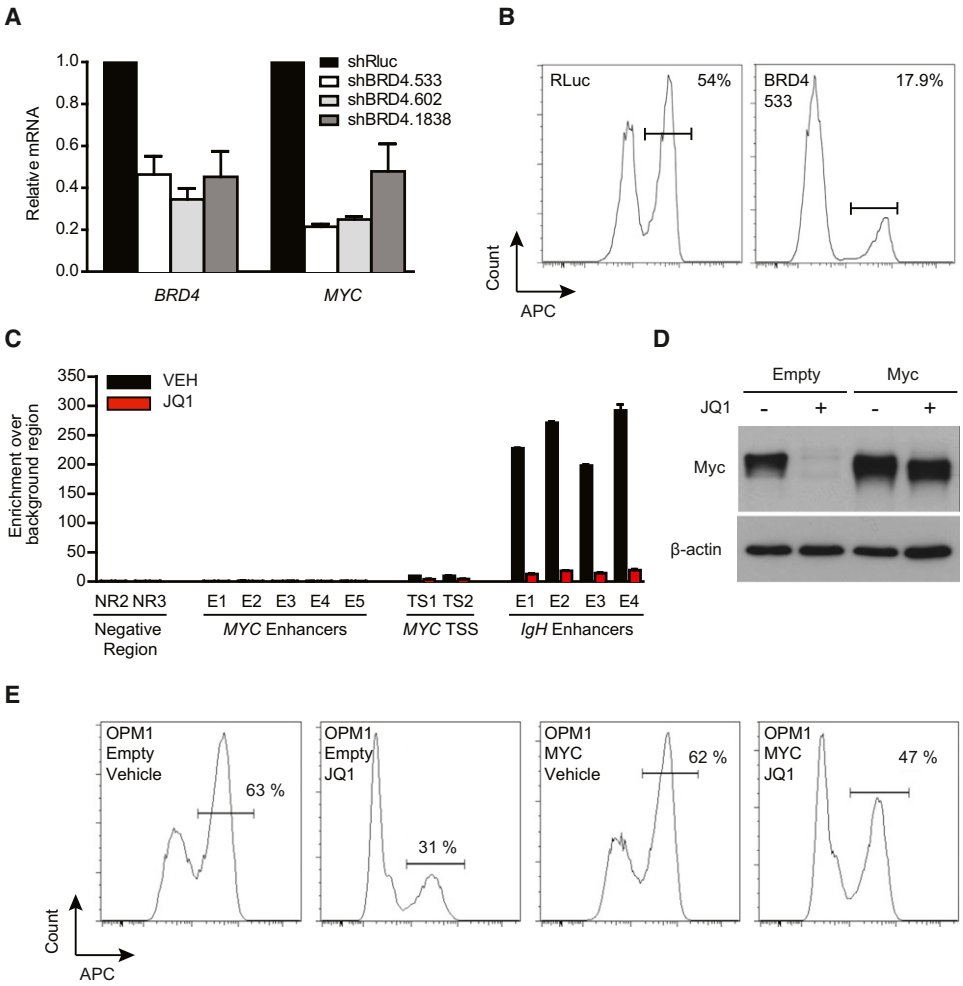

Figure 4. Regulation of *MYC* Transcription by BET Bromodomains

(A) *BRD4* and *MYC* expression in OPM1 cells transduced with either shBRD4 (three different hairpins) or a Renilla control hairpin (shRluc). shRNAs were induced for 5 days before analysis by qRT-PCR. Data normalized to GAPDH are presented as mean ± SEM of three biological replicates.

(B) Cell-cycle analysis of OPM1 cells transduced with the indicated shRNA for 6 days. BrdU staining (APC) identifies the fraction of cells in S phase. See also Figure S5.

(C) ChIP studies of BRD4 (anti-BRD4; Bethyl) binding to *MYC* TSS or proximal enhancers in MM.1S cells. Competitive displacement of BRD4 from IgH enhancers is observed upon treatment with JQ1 (500 nM for 24 hr, red bars) compared to vehicle control (black bars). Data represent mean ± SEM of three replicates. See also Figure S6.

(D) Immunoblotting of whole-cell lysates from empty MSCV vector- or Myc overexpression vector-transduced OPM1 cells after treating with JQ1 (500 nM, 24 hr) or DMSO control.

(E) Cell-cycle analysis of either empty or Myc-overexpressing OPM1 cells treated with JQ1 (500 nM, 24 hr). BrdU staining (APC) identifies the fraction of cells in S phase.

for the investigational study of BET bromodomain inhibitors in the treatment of MM.

DISCUSSION

Despite the centrality of Myc in the pathogenesis of cancer, conventional approaches toward direct Myc inhibition have not proven successful. To date, efforts to target c-Myc have identified only a small number of molecules with low biochemical potency and limited biological characterization (Bidwell et al., 2009; Hammoudeh et al., 2009; Jeong et al., 2010), underscoring both the challenge of targeting c-Myc as well as the enduring need for chemical probes of c-Myc transcriptional function. Considering chromatin as a platform for signal transduction

(H) Heatmap of clustered gene expression data from multiplexed measurement (Nanostring) of cancer-associated genes in three human MM cell lines treated with JQ1 or vehicle control. Among 230 genes studied (Figure S4), four genes (*MYC*, *TERT*, *TYRO3*, and *MYB*) exhibited statistically significant ($p < 0.05$) downregulation. Replicate expression measurements exhibited high concordance among low and highly expressed genes (Figure S3B).

(I) Immunoblotting study of four MM lines (KMS11, LR5, OPM1, and INA-6) identifies a JQ1-induced decrease in c-Myc expression (500 nM, 24 hr).

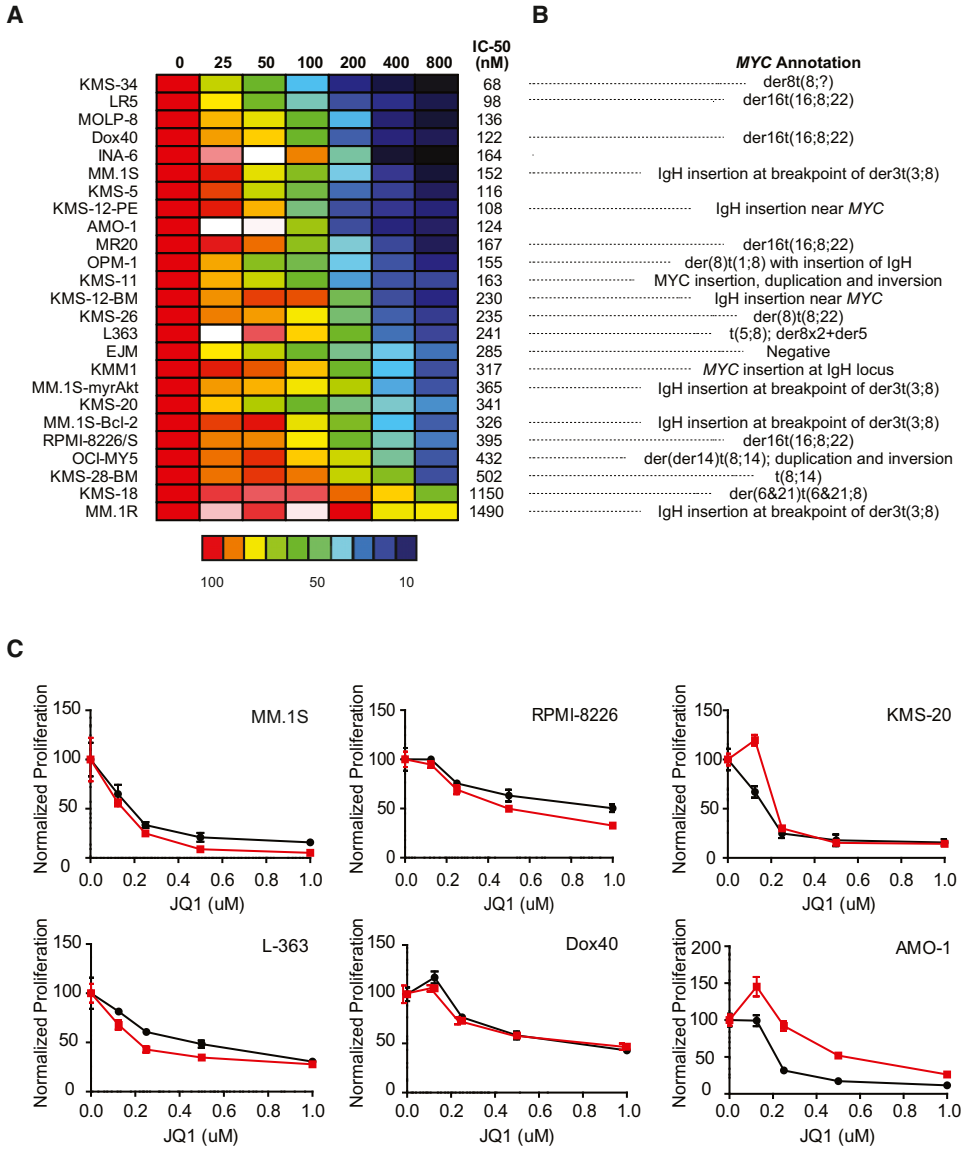

Figure 5. Antimyeloma Activity of JQ1 In Vitro

(A) A panel of MM cell lines was tested for in vitro sensitivity to JQ1 (12.5–800 nM, 72 hr) by measurement of ATP levels (Cell TiterGlo; Promega).

(B) *MYC* genomic status of selected MM cell lines from (A), as annotated (Dib et al., 2008).

(C) Activity of JQ1 against MM cell lines cultured in the presence (red lines) or absence (black lines) of the HS-5 stromal cell line, assessed by CS-BLI (McMillin et al., 2010). Data represent mean ± SD for four biological replicates.

(Schreiber and Bernstein, 2002), we have undertaken to inhibit Myc transcription and function through displacement of chromatin-bound, coactivator proteins using competitive small molecules. Using a first-in-class, small-molecule bromodomain inhibitor developed by our laboratories, JQ1, we validate BET bromodomains as determinants of c-Myc transcription and as therapeutic targets in MM, an ideal model system for the mechanistic and translational study of Myc pathway inhibitors.

Most importantly, we illustrate the feasibility of selectively downregulating transcription of *MYC* itself via the molecular action of a selective, small molecule. The ensuing suppression of c-Myc protein levels, depletion of chromatin-bound c-Myc, and concomitant downregulation of the Myc-dependent transcriptional network lead to growth-inhibitory effects sharing the specificity of phenotypes associated with prior genetic models of Myc inhibition. These are notable observations that distinguish the transcriptional consequences of BET inhibition from other nonselective transcriptional inhibitors, such as actinomycin D, α-amanitin, and flavopiridol.

A compelling finding is the observed, direct interaction of BRD4 with IgH enhancers in MM cells possessing IgH rearrangement into the *MYC* locus and the depletion of BRD4 binding by JQ1. This suggests BET inhibition as a strategy for targeting other structural rearrangements in cancer involving IgH or other

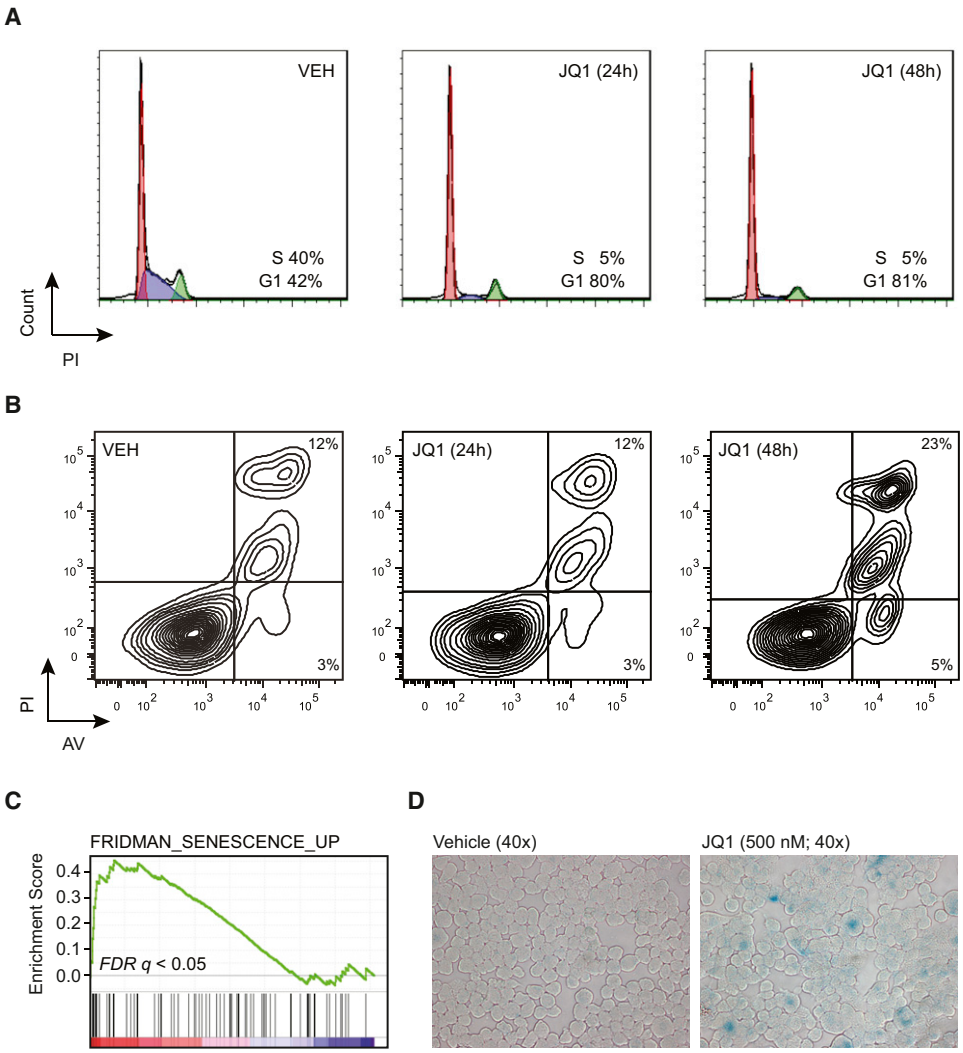

Figure 6. JQ1 Induces Cell-Cycle Arrest and Cellular Senescence in MM Cells

(A and B) Flow cytometric evaluation of propidium iodide (PI) staining for cell-cycle analysis (A) and detection of Annexin V-positive apoptotic cells (B) in JQ1-treated MM.1S cells (0–48 hr, 500 nM).

(C) Enrichment of senescence-associated genes among JQ1-suppressed genes in MM.1S cells.

(D) Induction of cellular senescence in JQ1-treated MM.1S cells (500 nM, 48 hr), as detected by β-galactosidase staining.

strong enhancers and has potential implications for the modulation of immunoglobulin gene expression in autoimmune diseases.

An unexpected finding was the pronounced and concordant suppression of multiple E2F-dependent transcriptional signatures. In this instance, *E2F1* protein and transcript levels were not affected by BET inhibition, suggesting either an unrecognized function of BET bromodomains in E2F transcriptional complexes or a dominant effect of Myc downregulation causing cell-cycle arrest in G1 leading to silencing of E2F. These observations are also compatible with the known role of Myc and E2F1 as transcriptional collaborators in cell-cycle progression and tumor cell survival (Matsumura et al., 2003; Trimarchi and Lees, 2002).

Insights provided by our study identify rational strategies for combination therapeutic approaches warranting exploration in MM. *MYC* activation is commonly accompanied by antiapoptotic signaling in human cancer. In MM, constitutive or microenvironment-inducible activation of antiapoptotic Bcl-2 proteins has been reported (Harada et al., 1998; Legartova et al., 2009). Thus, Myc pathway inhibition by JQ1 may demonstrate synergism with targeted proapoptotic agents (e.g., ABT-737) (Oltersdorf et al., 2005; Trudel et al., 2007). Additionally, the selective effect of JQ1 on Myc and E2F1 transcriptional programs provides an opportunity to combine BET inhibitors with pathway-directed antagonists of the NF-κB, STAT3, XBP1, or HSF1 transcriptional programs.

Direct inhibition of c-Myc remains a central challenge in the discipline of ligand discovery. Inhibition of *MYC* expression and function, demonstrated herein, presents an immediate opportunity to study and translate the concept of c-Myc inhibition more

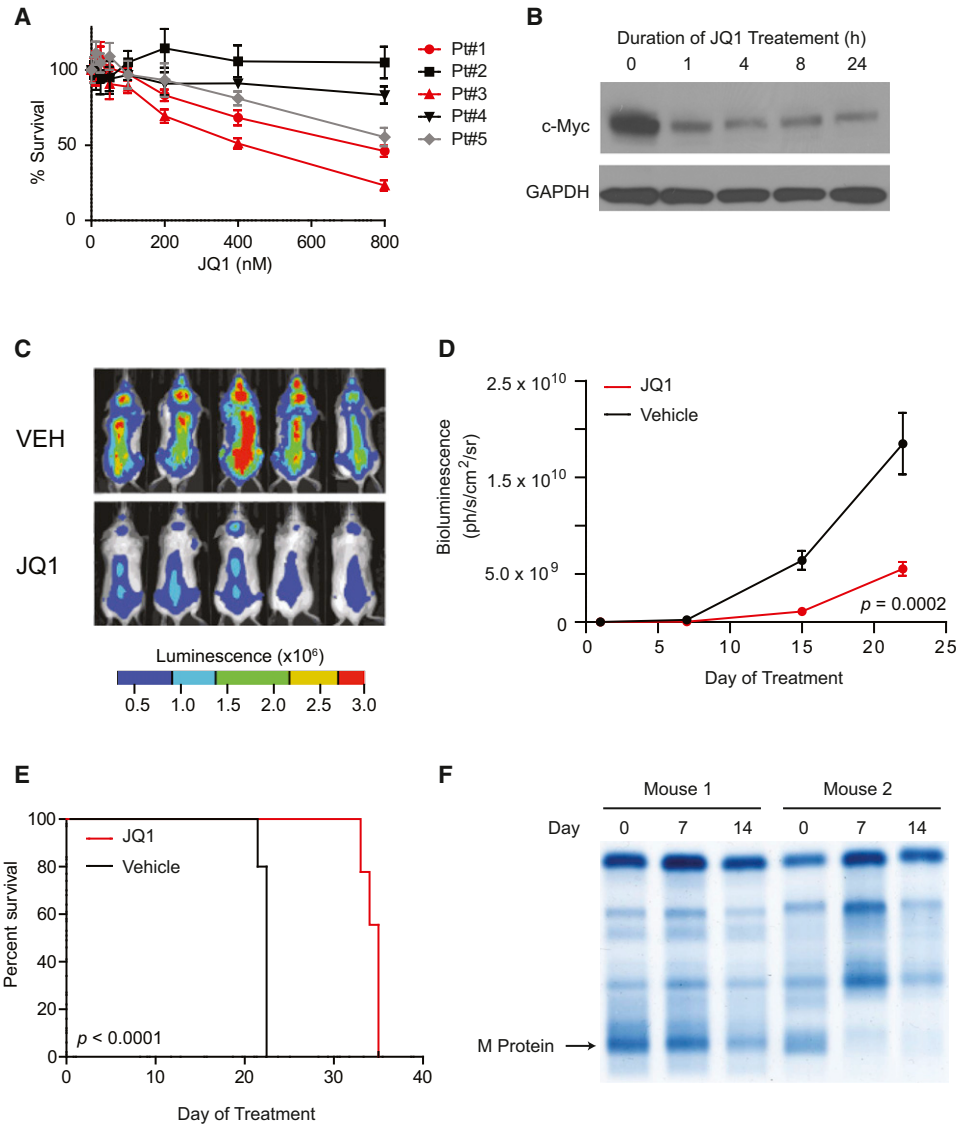

Figure 7. Translational Implications of BET Bromodomain Inhibition in MM

(A) JQ1 arrests the proliferation of primary, patient-derived CD138+ MM cells (Cell TiterGlo; Promega). Data represent the mean ± SD of four replicates per condition.

(B) c-Myc immunoblot shows JQ1-induced downregulation in short-term culture of primary, patient-derived MM cells (500 nM, duration as indicated).

(C) Representative whole-body bioluminescence images of SCID-beige mice orthotopically xenografted after intravenous injection with MM.1S-luc+ cells and treated with JQ1 (50 mg/kg IP daily) or vehicle control.

(D) Tumor burden of SCID-beige mice orthotopically xenografted after intravenous injection with MM.1S-luc+ cells. Upon detection of MM lesions diffusely engrafted in the skeleton, mice were randomly assigned to receive JQ1 (50 mg/kg IP daily) or vehicle control. Data are presented as mean ± SEM (n = 10/group).

(E) Survival curves (Kaplan-Meier) of mice with orthotopic diffuse MM lesions show prolongation of overall survival with JQ1 treatment compared to vehicle control (log-rank test, $p < 0.0001$).

(F) Serum protein electrophoresis to detect monoclonal, tumor-derived immunoglobulin (M-protein) in two MM-bearing Vk*myc mice before or after 7 and 14 days of JQ1 treatment. JQ1 treatment induced partial and complete responses, respectively, in mouse 1 and mouse 2.

See also Figure S7.

broadly in human cancer. During the course of this research, a collaborative effort with the laboratories of Christopher Vakoc and Scott Lowe revealed *BRD4* as a tumor dependency in acute myeloid leukemia. Consistent with our observations described here in MM, leukemia cells similarly require BRD4 to sustain *MYC* expression to enforce aberrant self-renewal (Zuber et al., 2011). Collectively, these findings highlight a broad role for BRD4 in maintaining *MYC* expression in diverse hematopoietic malignancies and suggest the utility of drug-like BET bromodomain inhibitors as therapeutic agents in these diseases.

EXPERIMENTAL PROCEDURES

Gene Expression Analysis

MM cells treated with JQ1 (500 nM, 24 h) were processed for transcriptional profiling using Affymetrix Human Gene 1.0 ST microarrays. Expression of individual genes was assessed in the context of dose- and time-ranging experiments by real-time quantitative polymerase chain reaction, multiplexed direct detection (Nanostring), and immunoblotting using antibodies as described in the Extended Experimental Procedures.

Chromatin Immunoprecipitation

ChIP was performed on MM.1S cells cultured in the presence or absence of JQ1 (500 nM, 24 hr). Specific antibodies, detailed methods, and primer sequences for MYC and IgH enhancers, as well as the MYC TSS, are described in the Extended Experimental Procedures.

In Vitro and In Vivo MM Studies

The impact of JQ1 on cell viability, proliferation, and cell cycle was assessed in human MM cells as documented in the Extended Experimental Procedures. In vivo efficacy studies were performed with protocols approved by Institutional Animal Care and Use Committees at the DFCI or Mayo Clinic Arizona. JQ1 was administered by intraperitoneal injection into SCID-beige mice with MM lesions established after subcutaneous or intravenous injections and in nonimmunocompromised tumor-bearing Vk*myc mice. Tumor burden in these models was quantified by caliper measurement, whole-body bioluminescence imaging, and serum protein electrophoresis, respectively, as detailed in the Extended Experimental Procedures.

ACCESSION NUMBERS

Oligonucleotide microarray data have been deposited in the Gene Expression Omnibus under the accession number GSE31365.

SUPPLEMENTAL INFORMATION

Supplemental Information includes Extended Experimental Procedures, seven figures, and one table and can be found with this article online at doi:10.1016/j.cell.2011.08.017.

ACKNOWLEDGMENTS

We are grateful to S. Lowe for sharing unpublished information; A. Azab, D. McMillin, C. Ott, and A. Roccaro for technical support; E. Fox for microarray data; J. Daley and S. Lazo-Kallanian for flow cytometry; the MMRF, MMRC, and Broad Institute for establishing the MM Genomics Portal (http://www.broadinstitute.org/mmgp/). This research was supported by NIH-K08CA128972 (J.E.B.), NIH-R01CA050947 (C.S.M.), NIH-R01HG002668 (R.A.Y.), and NIH-R01CA46455 (R.A.Y.); the Chambers Medical Foundation (P.G.R., C.S.M.); the Stepanian Fund for Myeloma Research (P.G.R., C.S.M.); and the Richard J. Corman Foundation (P.G.R., C.S.M.); an American Cancer Society Postdoctoral Fellowship, 120272-PF-11-042-01-DMC (P.B.R.); the Burroughs-Wellcome Fund, the Smith Family Award, the Damon-Runyon Cancer Research Foundation, and the MMRF (to J.E.B.).

J.E.B. and C.S.M. designed the study, analyzed data, and prepared the manuscript. J.E.D., H.M.J., and E.K. assayed MM drug sensitivity. G.C.I. and J.E.D. assessed the effects of JQ1 on Myc expression. J.Q. performed scaling synthesis and purification of JQ1. P.G.R. and K.C.A. provided primary MM samples. P.B.R. and T.G. conducted ChIP experiments, and P.B.R. and R.A.Y. contributed to their interpretation. R.M.P., T.P.H., and M.R.M. performed RNA expression analysis. I.M.G. and K.C.A. provided support and interpreted cellular data. A.C.S. and W.C.H. designed and performed shRNA screens. M.E.L. analyzed expression array data. J.S. and C.R.V. performed Myc rescue experiments. A.L.K. supervised in vivo efficacy and biostatistical studies. M.C. and P.L.B. performed in vivo GEMM studies. J.E.B. and C.S.M. supervised the research. All authors edited the manuscript.

Received: July 19, 2011
Revised: August 13, 2011
Accepted: August 15, 2011
Published online: September 1, 2011

REFERENCES

Amati, B., Brooks, M.W., Levy, N., Littlewood, T.D., Evan, G.I., and Land, H. (1993). Oncogenic activity of the c-Myc protein requires dimerization with Max. Cell *72*, 233–245.

Beroukhim, R., Mermel, C.H., Porter, D., Wei, G., Raychaudhuri, S., Donovan, J., Barretina, J., Boehm, J.S., Dobson, J., Urashima, M., et al. (2010). The landscape of somatic copy-number alteration across human cancers. Nature *463*, 899–905.

Bidwell, G.L., 3rd, Davis, A.N., and Raucher, D. (2009). Targeting a c-Myc inhibitory polypeptide to specific intracellular compartments using cell penetrating peptides. J. Control. Release *135*, 2–10.

Bisgrove, D.A., Mahmoudi, T., Henklein, P., and Verdin, E. (2007). Conserved P-TEFb-interacting domain of BRD4 inhibits HIV transcription. Proc. Natl. Acad. Sci. USA *104*, 13690–13695.

Blackwood, E.M., and Eisenman, R.N. (1991). Max: a helix-loop-helix zipper protein that forms a sequence-specific DNA-binding complex with Myc. Science *251*, 1211–1217.

Chapman, M.A., Lawrence, M.S., Keats, J.J., Cibulskis, K., Sougnez, C., Schinzel, A.C., Harview, C.L., Brunet, J.P., Ahmann, G.J., Adli, M., et al. (2011). Initial genome sequencing and analysis of multiple myeloma. Nature *471*, 467–472.

Chesi, M., Robbiani, D.F., Sebag, M., Chng, W.J., Affer, M., Tiedemann, R., Valdez, R., Palmer, S.E., Haas, S.S., Stewart, A.K., et al. (2008). AID-dependent activation of a MYC transgene induces multiple myeloma in a conditional mouse model of post-germinal center malignancies. Cancer Cell *13*, 167–180.

Chng, W.J., Huang, G.F., Chung, T.H., Ng, S.B., Gonzalez-Paz, N., Troska-Price, T., Mulligan, G., Chesi, M., Bergsagel, P.L., and Fonseca, R. (2011). Clinical and biological implications of MYC activation: a common difference between MGUS and newly diagnosed multiple myeloma. Leukemia *25*, 1026–1035.

Claudio, J.O., Masih-Khan, E., Tang, H., Gonçalves, J., Voralia, M., Li, Z.H., Nadeem, V., Cukerman, E., Francisco-Pabalan, O., Liew, C.C., et al. (2002). A molecular compendium of genes expressed in multiple myeloma. Blood *100*, 2175–2186.

Dang, C.V. (2009). MYC, microRNAs and glutamine addiction in cancers. Cell Cycle *8*, 3243–3245.

Dang, C.V., Le, A., and Gao, P. (2009). MYC-induced cancer cell energy metabolism and therapeutic opportunities. Clin. Cancer Res. *15*, 6479–6483.

Darnell, J.E., Jr. (2002). Transcription factors as targets for cancer therapy. Nat. Rev. Cancer *2*, 740–749.

Dean, M., Kent, R.B., and Sonenshein, G.E. (1983). Transcriptional activation of immunoglobulin alpha heavy-chain genes by translocation of the c-myc oncogene. Nature *305*, 443–446.

Dey, A., Nishiyama, A., Karpova, T., McNally, J., and Ozato, K. (2009). Brd4 marks select genes on mitotic chromatin and directs postmitotic transcription. Mol. Biol. Cell *20*, 4899–4909.

Dhalluin, C., Carlson, J.E., Zeng, L., He, C., Aggarwal, A.K., and Zhou, M.M. (1999). Structure and ligand of a histone acetyltransferase bromodomain. Nature *399*, 491–496.

Dib, A., Gabrea, A., Glebov, O.K., Bergsagel, P.L., and Kuehl, W.M. (2008). Characterization of MYC translocations in multiple myeloma cell lines. J. Natl. Cancer Inst. Monogr., 25–31.

Filippakopoulos, P., Qi, J., Picaud, S., Shen, Y., Smith, W.B., Fedorov, O., Morse, E.M., Keates, T., Hickman, T.T., Felletar, I., et al. (2010). Selective inhibition of BET bromodomains. Nature *468*, 1067–1073.

Frank, S.R., Parisi, T., Taubert, S., Fernandez, P., Fuchs, M., Chan, H.M., Livingston, D.M., and Amati, B. (2003). MYC recruits the TIP60 histone acetyltransferase complex to chromatin. EMBO Rep. *4*, 575–580.

Frye, S.V. (2010). The art of the chemical probe. Nat. Chem. Biol. *6*, 159–161.

Fukazawa, T., Maeda, Y., Matsuoka, J., Yamatsuji, T., Shigemitsu, K., Morita, I., Faiola, F., Durbin, M.L., Soucek, L., and Naomoto, Y. (2010). Inhibition of Myc effectively targets KRAS mutation-positive lung cancer expressing high levels of Myc. Anticancer Res. *30*, 4193–4200.

Gomi, M., Moriwaki, K., Katagiri, S., Kurata, Y., and Thompson, E.B. (1990). Glucocorticoid effects on myeloma cells in culture: correlation of growth inhibition with induction of glucocorticoid receptor messenger RNA. Cancer Res. *50*, 1873–1878.

Hammoudeh, D.I., Follis, A.V., Prochownik, E.V., and Metallo, S.J. (2009). Multiple independent binding sites for small-molecule inhibitors on the oncoprotein c-Myc. J. Am. Chem. Soc. *131*, 7390–7401.

Harada, N., Hata, H., Yoshida, M., Soniki, T., Nagasaki, A., Kuribayashi, N., Kimura, T., Matsuzaki, H., and Mitsuya, H. (1998). Expression of Bcl-2 family of proteins in fresh myeloma cells. Leukemia *12*, 1817–1820.

Harris, A.W., Pinkert, C.A., Crawford, M., Langdon, W.Y., Brinster, R.L., and Adams, J.M. (1988). The E mu-myc transgenic mouse. A model for high-incidence spontaneous lymphoma and leukemia of early B cells. J. Exp. Med. *167*, 353–371.

Haynes, S.R., Dollard, C., Winston, F., Beck, S., Trowsdale, J., and Dawid, I.B. (1992). The bromodomain: a conserved sequence found in human, Drosophila and yeast proteins. Nucleic Acids Res. *20*, 2603.

Hideshima, T., Mitsiades, C., Tonon, G., Richardson, P.G., and Anderson, K.C. (2007). Understanding multiple myeloma pathogenesis in the bone marrow to identify new therapeutic targets. Nat. Rev. Cancer *7*, 585–598.

Hurt, E.M., Wiestner, A., Rosenwald, A., Shaffer, A.L., Campo, E., Grogan, T., Bergsagel, P.L., Kuehl, W.M., and Staudt, L.M. (2004). Overexpression of c-maf is a frequent oncogenic event in multiple myeloma that promotes proliferation and pathological interactions with bone marrow stroma. Cancer Cell *5*, 191–199.

Jain, M., Arvanitis, C., Chu, K., Dewey, W., Leonhardt, E., Trinh, M., Sundberg, C.D., Bishop, J.M., and Felsher, D.W. (2002). Sustained loss of a neoplastic phenotype by brief inactivation of MYC. Science *297*, 102–104.

Jeong, K.C., Ahn, K.O., and Yang, C.H. (2010). Small-molecule inhibitors of c-Myc transcriptional factor suppress proliferation and induce apoptosis of promyelocytic leukemia cell via cell cycle arrest. Mol. Biosyst. *6*, 1503–1509.

Keats, J.J., Fonseca, R., Chesi, M., Schop, R., Baker, A., Chng, W.J., Van Wier, S., Tiedemann, R., Shi, C.X., Sebag, M., et al. (2007). Promiscuous mutations activate the noncanonical NF-kappaB pathway in multiple myeloma. Cancer Cell *12*, 131–144.

Kim, J., Chu, J., Shen, X., Wang, J., and Orkin, S.H. (2008). An extended transcriptional network for pluripotency of embryonic stem cells. Cell *132*, 1049–1061.

Kim, Y.H., Girard, L., Giacomini, C.P., Wang, P., Hernandez-Boussard, T., Tibshirani, R., Minna, J.D., and Pollack, J.R. (2006). Combined microarray analysis of small cell lung cancer reveals altered apoptotic balance and distinct expression signatures of MYC family gene amplification. Oncogene *25*, 130–138.

Leder, A., Pattengale, P.K., Kuo, A., Stewart, T.A., and Leder, P. (1986). Consequences of widespread deregulation of the c-myc gene in transgenic mice: multiple neoplasms and normal development. Cell *45*, 485–495.

Legartova, S., Krejci, J., Harnicarova, A., Hajek, R., Kozubek, S., and Bartova, E. (2009). Nuclear topography of the 1q21 genomic region and Mcl-1 protein levels associated with pathophysiology of multiple myeloma. Neoplasma *56*, 404–413.

Malo, N., Hanley, J.A., Cerquozzi, S., Pelletier, J., and Nadon, R. (2006). Statistical practice in high-throughput screening data analysis. Nat. Biotechnol. *24*, 167–175.

Matsumura, I., Tanaka, H., and Kanakura, Y. (2003). E2F1 and c-Myc in cell growth and death. Cell Cycle *2*, 333–338.

Mattioli, M., Agnelli, L., Fabris, S., Baldini, L., Morabito, F., Bicciato, S., Verdelli, D., Intini, D., Nobili, L., Cro, L., et al. (2005). Gene expression profiling of plasma cell dyscrasias reveals molecular patterns associated with distinct IGH translocations in multiple myeloma. Oncogene *24*, 2461–2473.

McMillin, D.W., Delmore, J., Weisberg, E., Negri, J.M., Geer, D.C., Klippel, S., Mitsiades, N., Schlossman, R.L., Munshi, N.C., Kung, A.L., et al. (2010). Tumor cell-specific bioluminescence platform to identify stroma-induced changes to anticancer drug activity. Nat. Med. *16*, 483–489.

Mitsiades, C.S., Mitsiades, N.S., McMullan, C.J., Poulaki, V., Shringarpure, R., Akiyama, M., Hideshima, T., Chauhan, D., Joseph, M., Libermann, T.A., et al. (2004). Inhibition of the insulin-like growth factor receptor-1 tyrosine kinase activity as a therapeutic strategy for multiple myeloma, other hematologic malignancies, and solid tumors. Cancer Cell *5*, 221–230.

Mitsiades, N., Mitsiades, C.S., Poulaki, V., Chauhan, D., Fanourakis, G., Gu, X., Bailey, C., Joseph, M., Libermann, T.A., Treon, S.P., et al. (2002). Molecular sequelae of proteasome inhibition in human multiple myeloma cells. Proc. Natl. Acad. Sci. USA *99*, 14374–14379.

Nair, S.K., and Burley, S.K. (2003). X-ray structures of Myc-Max and Mad-Max recognizing DNA. Molecular bases of regulation by proto-oncogenic transcription factors. Cell *112*, 193–205.

Nicodeme, E., Jeffrey, K.L., Schaefer, U., Beinke, S., Dewell, S., Chung, C.W., Chandwani, R., Marazzi, I., Wilson, P., Coste, H., et al. (2010). Suppression of inflammation by a synthetic histone mimic. Nature *468*, 1119–1123.

Oltersdorf, T., Elmore, S.W., Shoemaker, A.R., Armstrong, R.C., Augeri, D.J., Belli, B.A., Bruncko, M., Deckwerth, T.L., Dinges, J., Hajduk, P.J., et al. (2005). An inhibitor of Bcl-2 family proteins induces regression of solid tumours. Nature *435*, 677–681.

Palumbo, A.P., Pileri, A., Dianzani, U., Massaia, M., Boccadoro, M., and Calabretta, B. (1989). Altered expression of growth-regulated protooncogenes in human malignant plasma cells. Cancer Res. *49*, 4701–4704.

Pomerantz, M.M., Ahmadiyeh, N., Jia, L., Herman, P., Verzi, M.P., Doddapaneni, H., Beckwith, C.A., Chan, J.A., Hills, A., Davis, M., et al. (2009a). The 8q24 cancer risk variant rs6983267 shows long-range interaction with MYC in colorectal cancer. Nat. Genet. *41*, 882–884.

Pomerantz, M.M., Beckwith, C.A., Regan, M.M., Wyman, S.K., Petrovics, G., Chen, Y., Hawksworth, D.J., Schumacher, F.R., Mucci, L., Penney, K.L., et al. (2009b). Evaluation of the 8q24 prostate cancer risk locus and MYC expression. Cancer Res. *69*, 5568–5574.

Rahl, P.B., Lin, C.Y., Seila, A.C., Flynn, R.A., McCuine, S., Burge, C.B., Sharp, P.A., and Young, R.A. (2010). c-Myc regulates transcriptional pause release. Cell *141*, 432–445.

Rahman, S., Sowa, M.E., Ottinger, M., Smith, J.A., Shi, Y., Harper, J.W., and Howley, P.M. (2011). The Brd4 extraterminal domain confers transcription activation independent of pTEFb by recruiting multiple proteins, including NSD3. Mol. Cell. Biol. *31*, 2641–2652.

Schlosser, I., Hölzel, M., Hoffmann, R., Burtscher, H., Kohlhuber, F., Schuhmacher, M., Chapman, R., Weidle, U.H., and Eick, D. (2005). Dissection of transcriptional programmes in response to serum and c-Myc in a human B-cell line. Oncogene *24*, 520–524.

Schreiber, S.L., and Bernstein, B.E. (2002). Signaling network model of chromatin. Cell *111*, 771–778.

Schuhmacher, M., Kohlhuber, F., Hölzel, M., Kaiser, C., Burtscher, H., Jarsch, M., Bornkamm, G.W., Laux, G., Polack, A., Weidle, U.H., and Eick, D. (2001). The transcriptional program of a human B cell line in response to Myc. Nucleic Acids Res. *29*, 397–406.

Shaffer, A.L., Emre, N.C., Lamy, L., Ngo, V.N., Wright, G., Xiao, W., Powell, J., Dave, S., Yu, X., Zhao, H., et al. (2008). IRF4 addiction in multiple myeloma. Nature *454*, 226–231.

Shou, Y., Martelli, M.L., Gabrea, A., Qi, Y., Brents, L.A., Roschke, A., Dewald, G., Kirsch, I.R., Bergsagel, P.L., and Kuehl, W.M. (2000). Diverse karyotypic abnormalities of the c-myc locus associated with c-myc dysregulation and tumor progression in multiple myeloma. Proc. Natl. Acad. Sci. USA *97*, 228–233.

Soucek, L., Helmer-Citterich, M., Sacco, A., Jucker, R., Cesareni, G., and Nasi, S. (1998). Design and properties of a Myc derivative that efficiently homodimerizes. Oncogene *17*, 2463–2472.

Soucek, L., Jucker, R., Panacchia, L., Ricordy, R., Tatò, F., and Nasi, S. (2002). Omomyc, a potential Myc dominant negative, enhances Myc-induced apoptosis. Cancer Res. *62*, 3507–3510.

Stewart, T.A., Pattengale, P.K., and Leder, P. (1984). Spontaneous mammary adenocarcinomas in transgenic mice that carry and express MTV/myc fusion genes. Cell *38*, 627–637.

Trimarchi, J.M., and Lees, J.A. (2002). Sibling rivalry in the E2F family. Nat. Rev. Mol. Cell Biol. *3*, 11–20.

Trudel, S., Stewart, A.K., Li, Z., Shu, Y., Liang, S.B., Trieu, Y., Reece, D., Paterson, J., Wang, D., and Wen, X.Y. (2007). The Bcl-2 family protein inhibitor, ABT-737, has substantial antimyeloma activity and shows synergistic effect with dexamethasone and melphalan. Clin. Cancer Res. *13*, 621–629.

Vervoorts, J., Lüscher-Firzlaff, J.M., Rottmann, S., Lilischkis, R., Walsemann, G., Dohmann, K., Austen, M., and Lüscher, B. (2003). Stimulation of c-MYC transcriptional activity and acetylation by recruitment of the cofactor CBP. EMBO Rep. *4*, 484–490.

Wu, C.H., van Riggelen, J., Yetil, A., Fan, A.C., Bachireddy, P., and Felsher, D.W. (2007). Cellular senescence is an important mechanism of tumor regression upon c-Myc inactivation. Proc. Natl. Acad. Sci. USA *104*, 13028–13033.

Zeller, K.I., Jegga, A.G., Aronow, B.J., O'Donnell, K.A., and Dang, C.V. (2003). An integrated database of genes responsive to the Myc oncogenic transcription factor: identification of direct genomic targets. Genome Biol. *4*, R69.

Zhan, F., Barlogie, B., Arzoumanian, V., Huang, Y., Williams, D.R., Hollmig, K., Pineda-Roman, M., Tricot, G., van Rhee, F., Zangari, M., et al. (2007). Gene-expression signature of benign monoclonal gammopathy evident in multiple myeloma is linked to good prognosis. Blood *109*, 1692–1700.

Zuber, J., Shi, J., Wang, E., Rappaport, A.R., Herrmann, H., Sison, E.A., Magoon, D., Qi, J., Blatt, K., Wunderlich, M., et al. (2011). RNAi screen identifies Brd4 as a therapeutic target in acute myeloid leukaemia. Nature. Published online August 3, 2011. 10.1038/nature10334.

EXTENDED EXPERIMENTAL PROCEDURES

Reagents

MM cell lines used were KMS-34, LR5, MOLP-8, Dox40, INA-6, MM.1S, KMS-5, KMS-12-PE, AMO-1, MR20, OPM-1, KMS-11, KMS-12-BM, KMS-26, L363, EJM, KMM1, MM.1S-myrAkt, KMS-20, MM.1S-Bcl-2, RPMI-8226/S, OCI-MY5, KMS-28-BM, KMS-18, and MM.1R. All MM cell lines were cultured in RPMI 1640 supplemented with 10% fetal bovine serum, 2mM glutamine, penicillin (100 U/ml), streptomycin (50 μg/ml). Additionally, the INA-6 cell line was supplemented with IL-6 (5 ng/ml) and an additional 10% fetal bovine serum (final concentration of 20%). Assays were also carried out under these respective conditions. Long term culture of the MM cells occurred in a Thermo Fisher Scientific (Waltham, MA) water jacketed incubator at 37°C and 5% CO_2. The thieno-triazolo-1,4-diazepine JQ1 compound used in assays was synthesized as previously described (Filippakopoulos et al., 2010), and diluted in DMSO to a stock concentration (10 mM) and subsequently diluted to working concentrations as indicated for biological studies.

Copy Number and Gene Expression Analysis in Primary Samples and MM Cell Lines

Gene expression data from publicly available Gene Expression Omnibus (GEO) datasets (accession numbers GSE5900 and GSE2113) were downloaded and analyzed through Oncomine 4.4 (http://www.oncomine.com). Differences in log_2-transformed median-centered transcript levels between different groups of samples were evaluated by non-parametric Kruskal-Wallis one-way analysis of variance and Dunn's Multiple Comparison Test. Statistical analyses were performed with Prism 5 software (Graphpad). Copy number data for the human 19p13.1 locus that harbors *BRD4* were downloaded from the publicly available database of the Multiple Myeloma Genomics Portal (MMGP) (http://www.broad.mit.edu/mmgp) for primary samples from 254 MM patients and for 45 MM cell lines. Data were analyzed using the Integrative Genomics Viewer (IGV) analysis software incorporated into MMGP. Oligonucleotide microarray data on the aforementioned MM cell lines were also downloaded from the MMGP. Previously published oligonucleotide microarray data (McMillin et al., 2010), were analyzed to compare expression of BRD4 transcript in INA6 myeloma cells cultured in vitro in the presence versus absence of HS-5 bone marrow stromal cells.

Arrayed Lentiviral shRNA Screens

shRNA screens were performed in INA-6 cells in an arrayed format using Cell Titer-Glo (Promega) to assess proliferation/viability phenotypes as described(Boehm et al., 2007; Moffat et al., 2006). Screening data was normalized using the statistical B-Score as described (Malo et al., 2006), and further visualized in Spotfire DecisionSite.

Expression Analysis

MM.1S cells were treated with compound (JQ1 500 nM) or vehicle (DMSO < 0.2%). RNA extraction was done with TRIzol Reagent (Invitrogen, 15596-026). cDNA was reverse transcribed (Applied Biosystems, N808-0234) and subsequently underwent quantitative real time PCR (Applied Biosystems, N15597) on an Applied Biosystems 7500 Real-Time PCR system with mammalian Taqman probes from Applied Biosystems: GAPDH (Hs 02758991_g1), CDKN1A (Hs00355782_m1), and MYC (Hs00905030_m1) following the manufacturer's protocol. Analysis was performed on triplicate PCR data for each biological duplicate normalized to GAPDH.

Nanostring Data Analysis

RNA was extracted as previously mentioned and added to Nanostring reagents as per manufacturer's protocol. Sample counts were first corrected for background based on negative control counts. Negative and zero values were set to 1 and the data log2-transformed. Counts were then scaled sequentially to doped-in positive controls and to 5 housekeeping genes (GAPDH, TUBB, HPRT1, GUSB, CLTC). To ensure comparable distributions, scaled counts were then quantile normalized (Bolstad et al., 2003) across samples using the Bioconductor *limma* implementation in R (Smyth, 2005). Gene values for which fewer than 25% of samples had counts above background (i.e., expressed at a reliably detectable level) were excluded from further analysis. In the time series experiment, genes were also filtered for variation to exclude those with an interquartile range < 0.5. Filtered data were used for unsupervised hierarchical clustering. For the time series experiment, samples and genes were clustered by Euclidean distance to reveal similarities in absolute expression levels. For the cell line comparison, Spearman's Rank Correlation was used to cluster genes. In both cases, color is globally normalized with blue indicating smallest fold change relative to the mean time 0 value (time series) or lowest expression level (3 cell lines). Red denotes greatest fold change or highest expression. Statistical significance of expression changes (relative to mean time 0 for the time series and treated versus untreated for the cell lines) was determined relative to a normal distribution with mean and standard deviation calculated for each comparison separately.

Oligonucleotide Microarray Profiling and Gene Set Enrichment Analysis

MM.1S, OPM1 and KMS11 MM cells were treated with JQ1 (500 nM, 24 h), cells were harvested, RNA was extracted and then processed for oligonucleotide microarray profiling. Affymetrix Human Gene 1.0 ST arrays (Gene Omnibus Express accession number GSE31365) were processed using the rma function of the affy Bioconductor package (Bolstad et al., 2003; Irizarry et al., 2003a; Irizarry et al., 2003b), and batch-corrected by cell type using ComBat (Johnson et al., 2007). Gene sets were downloaded from the Broad Institute's MSigDB website (Subramanian et al., 2005). Gene set permutations were used to determine statistical enrichment of the gene sets using the signal-to-noise ratio of DMSO-treated versus JQ1-treated cells.

shRNA Knockdown for BRD4

OPM1 cells were retrovirally transduced with VSVG-pseudotyped LMS-shRNA expression vectors (Zuber et al.). The day of infection of the cells was designated as day 0. The fraction of GFP-positive cells after infection was > 95%. RNA was collected at day 4 or day5 and qRT-PCR was performed using the following primers for human BRD4: CCCCTCGTGGTGGTGAAG and GCTCGCTGCGGAT GATG; GAPDH: CCTGACCTGCCGTCTAGAAA and CTCCGACGCCTGCTTCAC; and MYC: AGGGATCGCGCTGAGTATAA and TGCCTCTCGCTGGAATTACT. All signals were calculated by using deltaCt method and were normalized to GAPDH.

MYC Overexpression Studies

OPM1 cells were transduced using a MSCV-PGK- Puro-IRES-GFP (MSCV-PIG) construct (Hemann et al., 2003), with murine c-Myc or empty vector. 98% of infected cells became GFP-positive. The infected cells were then treated with 500 nM JQ1 for 24 hr and processed for staining (BD, APC BrdU Flow Kit, #552598). Immunoblotting was performed to confirm Myc expression. Specifically, cells were lysed directly in Laemmli buffer. About 50,000 cell equivalents were loaded in each lane. Protein extracts were resolved by SDS-PAGE electrophoresis and transferred to nitrocellulose for blotting with anti-Myc antibody (Epitomics, #1472- 1) or anti-β-actin HRP antibody (Sigma, #A3854).

Chromatin Immunoprecipitation Methods

Approximately $1x10^8$ MM.1S cells were treated with 500 nM JQ1 or DMSO for 24 hr and cross-linked with 1.1% formaldehyde (10 X crosslink solution contains: 11% formaldehyde, 50 mM HEPES pH 7.3, 100 mM NaCl, 1 mM EDTA pH 8.0, 0.5 mM EGTA pH 8.0) followed by two washes with PBS. Cells were scraped and frozen in liquid nitrogen. Brd4 ChIP-PCR analysis was done following a published protocol (Rahl et al., 2010). In brief, 75 μl of Dynal magnetic beads (Sigma) were blocked with 0.5% BSA (w/v) in PBS. Magnetic beads were bound with 6.25 μg of Brd4 antibody (Bethyl Labs, A310-985A, lot A301-985A-1 or Sigma, HPA015055-100, lot A31530). Cross-linked cells were lysed with lysis buffer 1 (50 mM HEPES pH 7.3, 140 mM NaCl, 1 mM EDTA, 10% glycerol, 0.5% NP-40, and 0.25% Triton X-100) and washed with lysis buffer 2 (10 mM Tris-HCl pH 8.0, 200 mM NaCl, 1 mM EDTA pH 8.0 and 0.5 mM EGTA pH 8.0). Cells were resuspended and sonicated in lysis buffer 3 (50 mM Tris-HCl pH 7.5, 140 mM NaCl, 1 mM EDTA, 1 mM EGTA, 1% Triton X-100, 0.1% Na-deoxycholate, 0.1% SDS) for 10 cycles at 30 s each on ice (18 W) with 60 s on ice between cycles. Sonicated lysates were cleared and incubated overnight at 4°C with magnetic beads bound with antibody to enrich for DNA fragments bound by the indicated factor. Beads were washed three times with sonication buffer, one time with sonication buffer with 500 mM NaCl, one time with LiCl wash buffer (20 mM Tris pH 8.0, 1 mM EDTA, 250 mM LiCl, 0.5% NP-40, 0.5% Na-deoxycholate) and one time with TE. DNA was eluted in elution buffer. Cross-links were reversed overnight. RNA and protein were digested using RNase A and Proteinase K, respectively and DNA was purified with phenol chloroform extraction and ethanol precipitation.

Brd4 ChIP and input DNA were analyzed using SYBR Green real-time PCR analysis (Applied Biosystems). ENCODE H3K27Ac ChIP-seq data available on the UCSC genome browser (http://genome.ucsc.edu/ENCODE/) was used to identify potential tissue-specific *MYC* enhancer and *IGH* enhancer regulatory elements and oligos were designed for these regions. Fold enrichment was determined from triplicate PCR reactions at five potential enhancer regions adjacent to the *MYC* gene in non-translocated cells (MYC_E1, MYC_E2, MYC_E3, MYC_E4, MYC_E5), the *MYC* transcriptional start site (MYC_TS1, MYC_TS2), *IGH* enhancer regions (IGH_E1, IGH_E2, IGH_E3, IGH_E4), and two negative regions upstream of the *MYC* enhancers (MYC_NR2, MYC_NR3) over input DNA using ΔΔCt over the negative region MYC_NR1. The oligos used for this analysis are listed in Table S1.

Immunoblotting

Lysates for blotting were prepared by seeding $5x10^6$ of the MM cells onto 100x20 mm tissue culture dish and JQ1 was added, at a final concentration of 500 nM for various time points. After collecting the cells the pellets were washed 3x with ice-cold 1X PBS and the pellet after the final wash was resuspended in lysis buffer containing Triton X-100, 50 mM Tris HCl (pH = 8.0), 120 mM NaCl, 5 mM EDTA, 1% Igepal, protease inhibitors (Roche Diagnostics, Indianapolis, IN), and phosphatase inhibitors (Calbiochem, Darmstadt, Germany). Protein concentrations were determined by using the Bradford reagent (Sigma-Aldrich, St. Louis, MO) and divided into 20 μg aliquots each containing LDS sample buffer (Invitrogen, Carlsbad, CA), and a reducing agent (Invitrogen, Carlsbad, CA). Samples were loaded into a NuPAGE Bis-Tris Gel (Invitrogen, Carlsbad, CA) and separated by electrophoreses at 200 V. The gels were then transferred onto a PVDF membrane (Immobilon-P; Millipore, Billerica, MA) by a wet transfer system (Invitrogen, Carlsbad, CA) and blocked by incubation with 5% dry milk in TBST (TBS with 0.2% Tween20). Membranes were probed using antibodies raised against c-*myc* (with concordant results obtained with different antibodies, including 9402 (Cell Signaling Technologies, Danvers, MA), 9E10, or sc-764 (Santa Cruz Biotechnology)), β-actin (Santa Cruz Biotechnology, SC-1616), GAPDH (Santa Cruz Biotechnology, SC-47724), and α-tubulin (Santa Cruz Biotechnology, SC-5286). Chemiluminescent detection was performed with appropriate secondary antibodies.

Transcription Factor DNA Binding Activity Assays

NFkB, c-Myc, and AP-1 transcription factor DNA binding ELISA assays (Active Motif, Carlsbad, CA) were carried out according to the manufacturer's instructions. In brief, 2-10 μg of MM1S nuclear lysates was added to an appropriate number of wells in the assay plate and the appropriate transcription factors were allowed to bind to its respective consensus sequence. Bound protein was then probed

with a primary antibody, washed to remove unbound protein, and finally probed with a secondary antibody conjugated to HRP. After a final wash, developing solution was added to each well and absorbance was measured on a spectrophotometer (Molecular Devices, Sunnyvale, California) at a wavelength of 450 nm (reference wavelength of 655 nm).

Nuclear Fractionation

The MM cell line MM.1S was seeded (5×10^6) onto a 100 × 20 mm tissue culture dish and JQ1 was added, at a final concentration of 500 nM, for 0.5, 1, 2, 4, 8, and 24 hr. All assay conditions were collected on ice at the longest duration time. Cells were washed twice with ice-cold 1 X PBS and after the final wash 1 ml of a buffer containing 10 mM HEPES, 350 mM sucrose, 5 mM EDTA, 1 mM PMSF, and protease inhibitors (Roche Diagnostics, Indianapolis, IN) was added to the cell pellet. Cells were homogenized with a B type Dounce homogenizer (10 strokes) and centrifuged at 1000 g for 10 min at 4°C. The supernatant was then discarded and the pellets containing the nuclear cell fraction were then lysed in buffer containing 50 mM Tris HCl (pH = 8.0), 120 mM NaCl, 5 mM EDTA, 1% Igepal, protease inhibitors (Roche Diagnostics, Indianapolis, IN), and phosphatase inhibitors (Calbiochem, Darmstadt, Germany). Protein concentration was determined by Bradford reagent (Sigma-Aldrich, St. Louis, MO) and protein was aliquoted according to transcription factor binding ELISA kit instructions.

Cell Viability Assays

MM cell lines were seeded onto 384-well tissue culture treated plates at a density of 1,000 cells/well in a volume of 50 μl of media. After seeding cells were incubated for 1 hr and during the interim a stock plate of JQ1 was thawed at room temperature in a desiccated box. The addition of JQ1 to the assay plate was done with disposable 384-well pins (V&P Scientific, San Diego, CA) that delivered 100 nL of the drug diluted in DMSO to each well of the plate. After 72 hr of incubation cells were analyzed for cell viability by the addition of CellTiter Glo (Promega, Madison, WI) to the assay plates. After 30 min incubation at 37°C the signal from the viable cells was analyzed on a Luminoskan luminometer (Labsystems Franklin, MA).

Compartment-Specific Bioluminescence Imaging for Stromal Coculture Studies

Similarly to published studies (McMillin et al., 2010), the immortalized HS-5 bone marrow stromal cell line was plated at a density of 2000 cells/well in a 384-well tissue culture treated plate at Day 0. MM cell lines stably transduced with luciferase constructs were then seeded Day +1 either in the presence or absence of HS-5 and incubated at 37°C for 1 hr prior to compound addition. At Day +4 cell viability was measured by the addition of luciferin (250 μg/mL) and final analysis on a Luminoskan luminometer (Labsystems Franklin, MA). Viability was assessed by comparing each condition to their respective drug free controls.

Flow Cytometric Studies

For cell cycle analyses, MM.1S cells ($10x10^5$ cell/mL) were treated with compound (JQ1 500 nM) or vehicle (DMSO < 0.2%) for 24 and 48 hr. Cells were spun down at 4°C, washed with PBS, fixed with 70% ethanol overnight, and washed with PBS. RNA was degraded with RNAase (Roche, 11579681001) and DNA was stained with propidium iodide. Samples were analyzed on a BD FACS Canto II. Histograms were generated and cell cycle analysis was performed using FlowJo flow cytometry analysis software (Tree Star, Inc.).

For apoptosis/necrosis detection, MM.1S cells (10×10^5 cell/mL) were treated with compound (JQ1 500 nM) or vehicle (DMSO < 0.2%) for 24 and 48 hr. The cells were washed and resuspended in Annexin-V/propidium iodide buffer solution containing Annexin V-FITC (BD Pharmigen, 51-66211e) and Propidium Iodide (BD Pharmigen, 51-65874x). Samples were immediately analyzed on a BD FACS Canto II. Visualizations and analyses of apoptotic fractions were generated using FlowJo flow cytometry analysis software (Tree Star, Inc.).

Cellular Senescence Staining

MM.1S cells were passaged with fresh media and into a four-chamber polystyrene vessel tissue culture treated glass slides (BD Falcon) to a seeding density of 2×10^5 cells per mL, and a final chamber volume of 500 μL. During passage, cells treated with compound (JQ1 500 nM) or vehicle (DMSO < 0.2%). After 48 hr the cells were stained for senescence using a β-Galactosidase Staining Kit (Cell Signaling Technology), and mounted for histology with 70% glycerol.

In Vivo Xenograft Studies

Five week old female SCID-beige mice were obtained from Charles River Labs (Wilmington, MA), and were acclimated one week prior to tumor cell inoculation. A total of 5×10^6 MM1S-LucNeo cells were injected subcutaneously, or 2×10^6 cells were injected via the lateral tail vein. Mice were imaged after injection of 75 mg/kg of D-luciferin (Promega, Madison, WI) using a Xenogen IVIS Spectrum (Caliper Life Sciences, Hopkinton, MA). Two weeks after inoculation, mice with established disease were divided into treatment groups (n = 10 per group). Mice were treated daily with either JQ1 at 50 mg/kg IP or vehicle (D5W) control. Tumor burden was assessed by serial bioluminescence imaging, or tumor volume measurements in the subcutaneous tumors. Bioluminescence was quantified using the Living Images software package (Caliper Life Sciences), and statistical significance was determined by Student's t test (and confirmed with non-parametric Mann-Whitney test). In the disseminated disease model statistical significance of survival differences was determined by log-rank test. Studies were performed under the auspices of protocols approved by the DFCI IACUC.

In Vivo Studies on Vk*MYC Mice

Vk*MYC mice (Chesi et al., 2008) were periodically bled by tail grazing. Blood was collected into Microtainer tubes (Becton Dickinson) and was let to coagulate at room temperature, before centrifugation for 10 min at 2,300 g. Sera were diluted 1:2 in normal saline buffer and analyzed by serum protein electrophoresis (SPEP) on a QuickGel Chamber apparatus using pre-casted QuickGels (Helena Laboratories) according to manufacturer's instruction. Densitometric analysis of the SPEP traces was performed using the clinically certified Helena QuickScan 2000 workstation, allowing a precise quantification of the various serum fractions, including the measurements of gamma/albumin ratio. Aged Vk*MYC mice with a M-spike of at least 15 g/L were treated intra-peritoneally for 5 days/week with JQ1 in 10% cyclodextrine (Sigma). SPEP was performed weekly and drug response was calculated by dividing the gamma/albumin ratio at d0 for each individual M-spike by the gamma/albumin ratio obtained post treatment. Densitometric profiles obtained at Day 0 and Day 14 were overlaid to show M-spike reduction.

SUPPLEMENTAL REFERENCES

Boehm, J.S., Zhao, J.J., Yao, J., Kim, S.Y., Firestein, R., Dunn, I.F., Sjostrom, S.K., Garraway, L.A., Weremowicz, S., Richardson, A.L., et al. (2007). Integrative genomic approaches identify IKBKE as a breast cancer oncogene. Cell *129*, 1065–1079.

Bolstad, B.M., Irizarry, R.A., Astrand, M., and Speed, T.P. (2003). A comparison of normalization methods for high density oligonucleotide array data based on variance and bias. Bioinformatics *19*, 185–193.

Chesi, M., Robbiani, D.F., Sebag, M., Chng, W.J., Affer, M., Tiedemann, R., Valdez, R., Palmer, S.E., Haas, S.S., Stewart, A.K., et al. (2008). AID-dependent activation of a MYC transgene induces multiple myeloma in a conditional mouse model of post-germinal center malignancies. Cancer Cell *13*, 167–180.

Filippakopoulos, P., Qi, J., Picaud, S., Shen, Y., Smith, W.B., Fedorov, O., Morse, E.M., Keates, T., Hickman, T.T., Felletar, I., et al. (2010). Selective inhibition of BET bromodomains. Nature *468*, 1067–1073.

Hemann, M.T., Fridman, J.S., Zilfou, J.T., Hernando, E., Paddison, P.J., Cordon-Cardo, C., Hannon, G.J., and Lowe, S.W. (2003). An epi-allelic series of p53 hypomorphs created by stable RNAi produces distinct tumor phenotypes in vivo. Nat. Genet. *33*, 396–400.

Irizarry, R.A., Bolstad, B.M., Collin, F., Cope, L.M., Hobbs, B., and Speed, T.P. (2003a). Summaries of Affymetrix GeneChip probe level data. Nucleic Acids Res. *31*, e15.

Irizarry, R.A., Hobbs, B., Collin, F., Beazer-Barclay, Y.D., Antonellis, K.J., Scherf, U., and Speed, T.P. (2003b). Exploration, normalization, and summaries of high density oligonucleotide array probe level data. Biostatistics *4*, 249–264.

Johnson, W.E., Li, C., and Rabinovic, A. (2007). Adjusting batch effects in microarray expression data using empirical Bayes methods. Biostatistics *8*, 118–127.

Malo, N., Hanley, J.A., Cerquozzi, S., Pelletier, J., and Nadon, R. (2006). Statistical practice in high-throughput screening data analysis. Nat. Biotechnol. *24*, 167–175.

McMillin, D.W., Delmore, J., Weisberg, E., Negri, J.M., Geer, D.C., Klippel, S., Mitsiades, N., Schlossman, R.L., Munshi, N.C., Kung, A.L., et al. (2010). Tumor cell-specific bioluminescence platform to identify stroma-induced changes to anticancer drug activity. Nat. Med. *16*, 483–489.

Moffat, J., Grueneberg, D.A., Yang, X., Kim, S.Y., Kloepfer, A.M., Hinkle, G., Piqani, B., Eisenhaure, T.M., Luo, B., Grenier, J.K., et al. (2006). A lentiviral RNAi library for human and mouse genes applied to an arrayed viral high-content screen. Cell *124*, 1283–1298.

Rahl, P.B., Lin, C.Y., Seila, A.C., Flynn, R.A., McCuine, S., Burge, C.B., Sharp, P.A., and Young, R.A. (2010). c-Myc regulates transcriptional pause release. Cell *141*, 432–445.

Smyth, G.K. (2005). Limma: linear models for microarray data. In Bioinformatics and Computational Biology Solutions using R and Bioconductor, R. Gentleman, V. Carey, S. Dudoit, R. Irizarry, and W. Huber, eds. (New York: Springer).

Subramanian, A., Tamayo, P., Mootha, V.K., Mukherjee, S., Ebert, B.L., Gillette, M.A., Paulovich, A., Pomeroy, S.L., Golub, T.R., Lander, E.S., and Mesirov, J.P. (2005). Gene set enrichment analysis: a knowledge-based approach for interpreting genome-wide expression profiles. Proc. Natl. Acad. Sci. USA *102*, 15545–15550.

Zuber, J., Rappaport, A.R., Luo, W., Wang, E., Chen, C., Vaseva, A.V., Shi, J., Weissmueller, S., Fellman, C., Taylor, M.J., et al. (2011). An integrated approach to dissecting oncogene addiction implicates a Myb-coordinated self-renewal program as essential for leukemia maintenance. Genes Dev. *25*, 1628–1640.

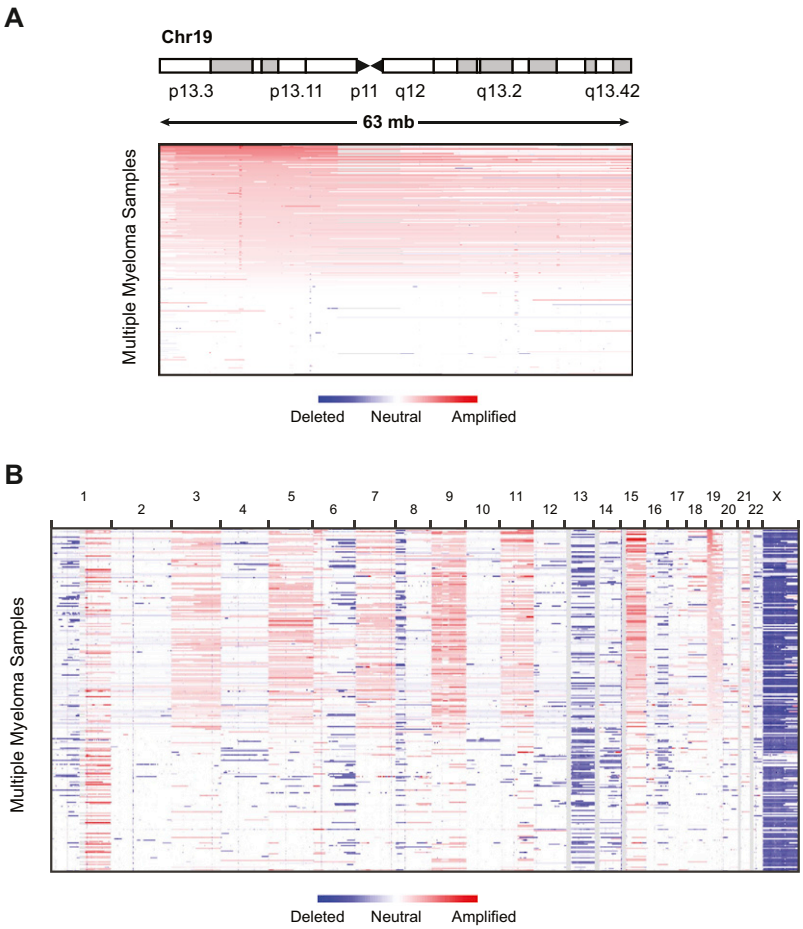

Figure S1. Amplification of the *BRD4* Locus in MM Samples, Related to Figure 1

(A) Copy number analysis of human chromosome 19 in primary samples from human MM patients (n = 254).

(B) Global view of genome-wide copy number changes in primary samples from human MM patients. Chromosome 19, which encodes BRD4 at Chr 19p.13.1, is amplified in the majority of MM patients.

A

Rank	MSigDB Gene Set	NES	FDR q-val
1	SGCGSSAAA_V$E2F1DP2_01	-2.25	< 0.00001
2	V$E2F1_Q6_01	-2.20	< 0.00001
3	V$E2F_02	-2.16	< 0.00001
4	V$E2F1_Q6	-2.16	< 0.00001
5	V$E2F1DP1_01	-2.15	< 0.00001
6	V$E2F1DP2_01	-2.15	< 0.00001
7	V$E2F4DP2_01	-2.14	< 0.00001
8	V$E2F_Q6	-2.11	< 0.00001
9	V$E2F_Q4	-2.09	< 0.00001
10	V$E2F4DP1_01	-2.09	< 0.00001
11	V$MYCMAX_01	-2.08	< 0.00001
12	V$E2F1_Q4_01	-2.07	< 0.00001
13	V$E2F_Q4_01	-2.05	< 0.00001
14	V$E2F_Q3_01	-2.03	< 0.00001
15	V$E2F_Q6_01	-2.02	< 0.00001
16	V$E2F1DP1RB_01	-1.98	< 0.00001
17	KTGGYRSGAA_UNKNOWN	-1.97	< 0.00001
18	V$E2F_03	-1.92	0.00004
19	V$NMYC_01	-1.90	0.0001
20	V$E2F1_Q3	-1.85	0.00036
21	V$E2F_Q3	-1.79	0.0011
22	V$USF_C	-1.78	0.0013
23	V$E2F_01	-1.74	0.0026
24	V$MYCMAX_02	-1.73	0.0027
25	V$MYCMAX_B	-1.64	0.0095
26	V$MYC_Q2	-1.63	0.011
27	V$E2F1_Q4	-1.62	0.013
28	V$MAX_01	-1.61	0.013

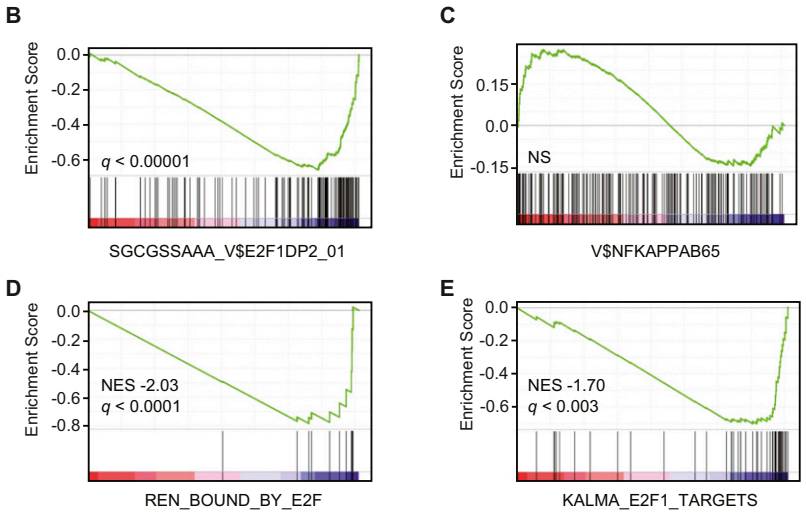

Figure S2. GSEA Analyses of Transcription Factor Target Gene Sets, Related to Figure 2

(A) Results of GSEA analysis for transcription factor target gene sets emerging with statistically significant enrichment among JQ1 downregulated genes.

(B and C) Enrichment of genes defined by gene sets for targets of (B) E2F1 and (C) NF-κB in JQ1-treated MM cells. E2F1 target genes are downregulated by JQ1 compared to NFkB genes, which are comparatively unaffected.

(D and E) GSEA documents that JQ1 treatment in MM cells also downregulates functionally defined gene sets for E2F.

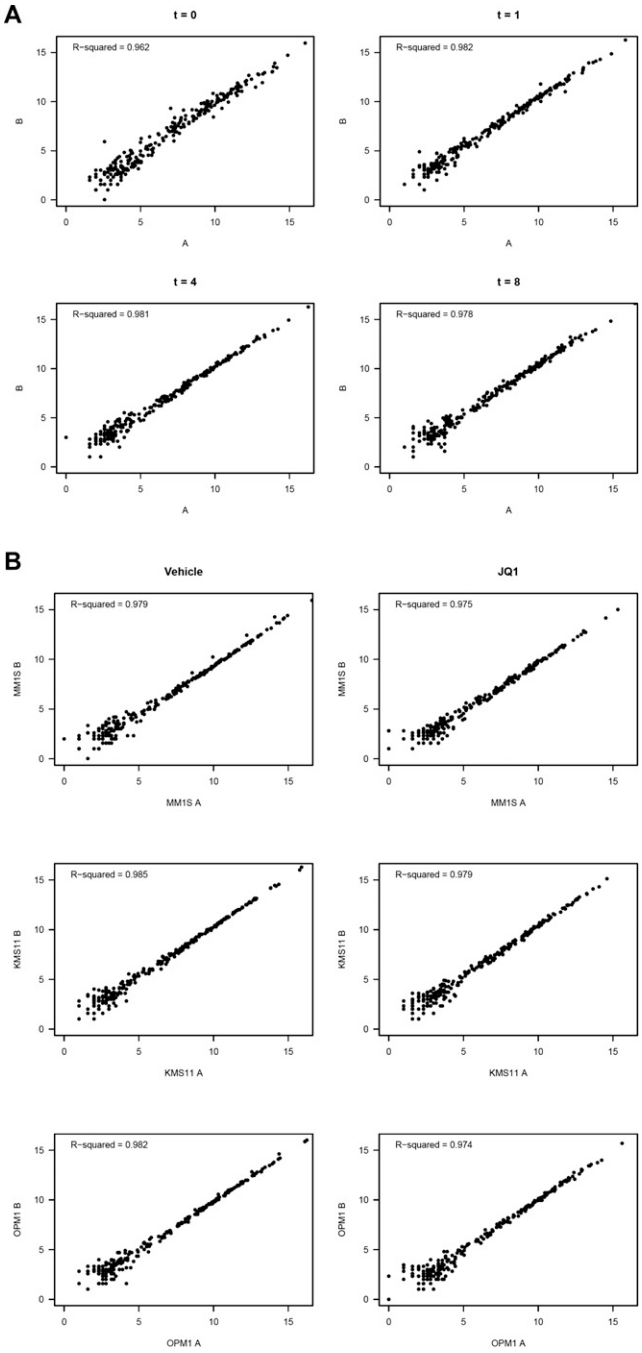

Figure S3. Concordance of Multiplexed Expression Data across Biological Replicates, Related to Figure 3

(A) Scatterplots of multiplexed expression data between biological replicates for MM.1S cells treated with JQ1 in a time-dependent manner (0-8hrs). R^2 values were calculated based on Pearson correlation coefficient. Average data for each transcript are presented as a heatmap in Figure 3.

(B) Scatterplots of multiplexed expression data between biological replicates for three MM cell lines (KMS11, MM.1S, OPM1) treated with JQ1 for 24 hr. R^2 values were calculated based on Pearson correlation coefficient. Replicate expression measurements exhibited high concordance among low and highly expressed genes. Average data for each transcript are presented as a heatmap in Figure S5B.

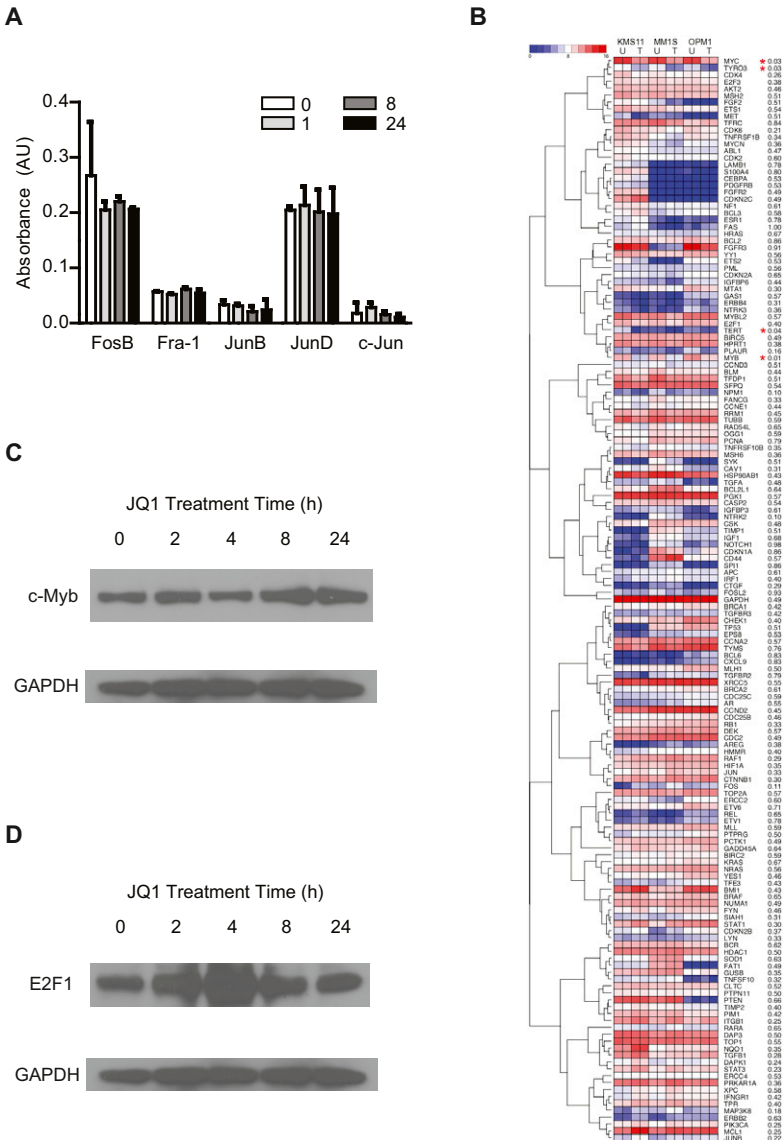

Figure S4. Myc-Specific Consequences of JQ1 Treatment, Related to Figure 3

(A) ELISA-based DNA binding assays document that JQ1 treatment (500 nM, 0 - 24 h) does not significantly affect the binding of AP-1 family members to consensus DNA binding sites. Data represent mean ± SEM.

(B) Gene expression profiling, by multiplexed transcriptional analysis, of three MM cell lines (KMS11, MM.1S and OPM1) treated with JQ1. MM cells were treated with JQ1 (500 nM) for 24 hr and assessed for effects on transcription of 230 cancer-related genes. Data are represented as a heatmap, with upregulated (red) and downregulated (blue) genes analyzed for statistical significant changes in expression. Maximum p-values of statistical significance of difference in JQ1-compared to vehicle-treated cells in all three lines are indicated. Asterisks denote genes (also presented in Figure 3H) demonstrating a statistically significant change in expression across all 3 cell lines.

(C and D) Immunoblotting analyses of (C) c-Myb and (D) E2F1 protein abundance in MM.1S cells following JQ1 treatment (0 - 24hrs, 500 nM). Measurement of GAPDH levels served as loading control.

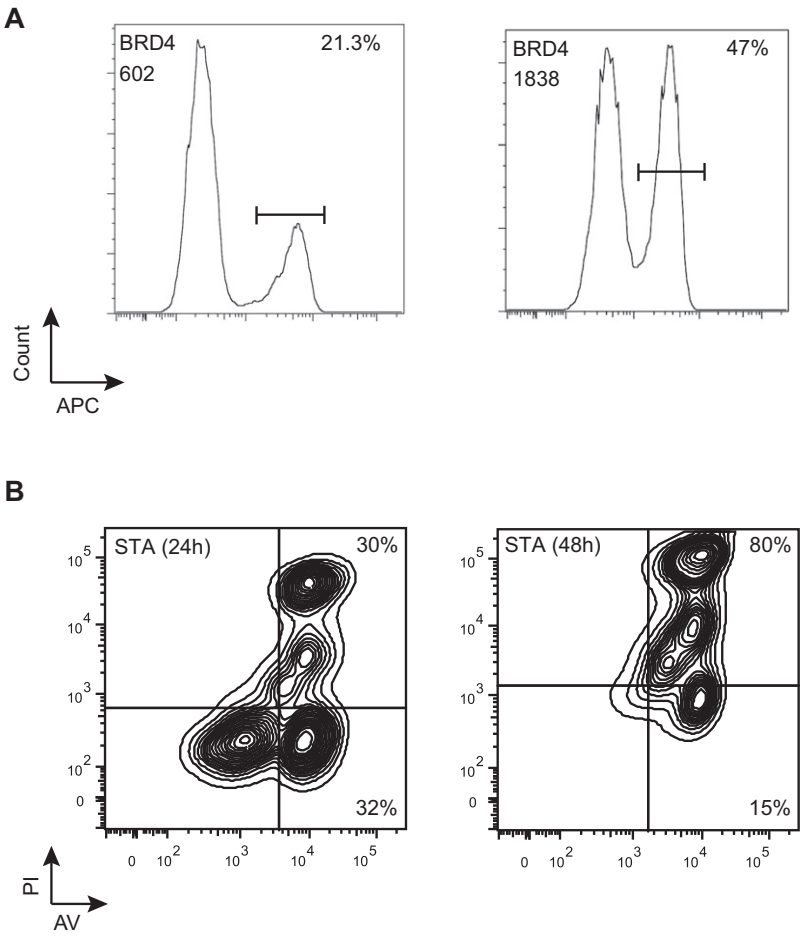

Figure S5. Flow Cytometry in MM Cells Infected with shRNA or Treated with Staurosporine, Related to Figure 4

(A) Cell cycle analysis of OPM1 cells transduced with the indicated shRNAs against BRD4 (shBRD4.602 and shBRD4.1838) for 6 days. BrdU staining (APC) indicates the percentage of S-phase cells. Notably, shBRD4.1838 produces less efficient suppression of *MYC* transcription, and exhibits a diminished effect on suppressing S-phase and cell cycle progression. These data support the role of MYC suppression by genetic (shRNA) or chemical (JQ1) inhibition of BET bromdomains.

(B) Induction of apoptosis by the non-selective kinase inhibitor staurosporine in MM.1S cells (500 nM for 24 or 48 hr, as indicated). Flow cytometry was performed using PI and Annexin V staining as described in Expanded Experimental Procedures.

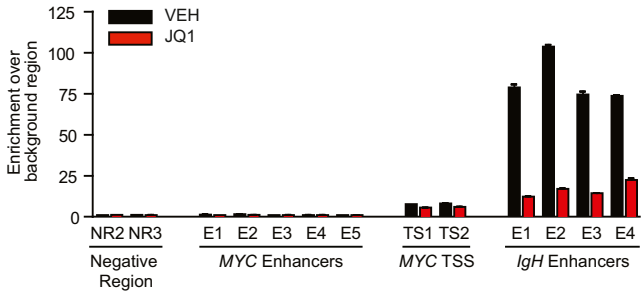

Figure S6. Chromatin Immunoprecipitation Studies of BRD4 Binding to MYC Promoter and Enhancer Regions, Related to Figure 4

Validation of BRD4 localization to the *IgH* enhancers (and, to a lesser extent, *MYC* TSS) is provided with a second independent antibody (anti-BRD4; Sigma). JQ1 demonstrates competitive inhibition of BRD4 binding to chromatin by ChIP, consistent with data presented in Figure 4C. Data represent mean ± SEM of three biological replicates.

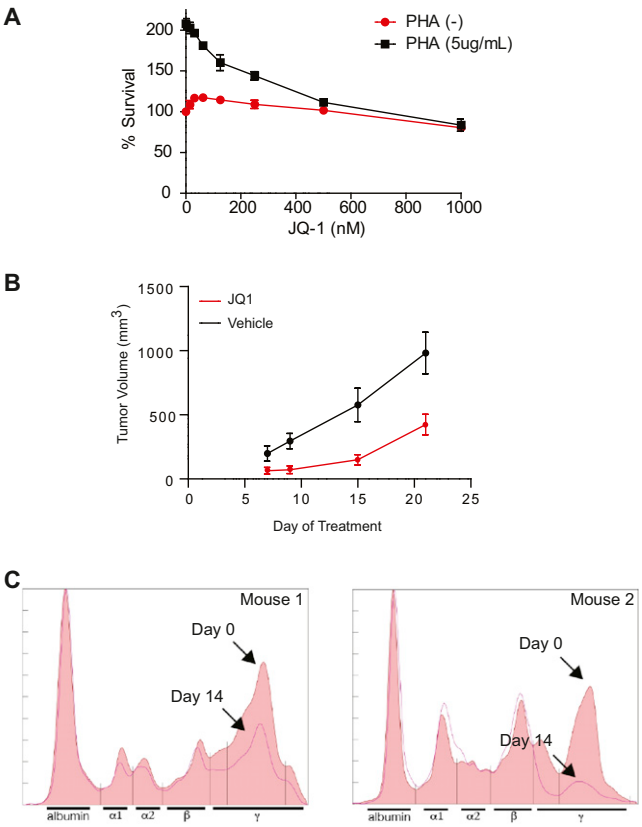

Figure S7. Efficacy of BET Inhibition with JQ1 in Murine Models of MM, Related to Figure 7

(A) BET inhibition with JQ1 has no effect on the viability of resting peripheral blood mononuclear cells (PBMCs) from normal donors (500 nM of JQ1 for 72 hr). Following PHA stimulation (5 μg/mL), a decrease in cellular proliferation was observed, supporting a selective effect of JQ1 treatment on proliferating cells. Data represent the mean ± SEM of three replicates per condition.

(B) Tumor burden (based on caliper measurements) of SCID-beige mice subcutaneously xenografted with MM.1S-luc+ cells. Upon detection of engrafted tumors, mice were randomly assigned to receive JQ-1 (50 mg/kg IP daily) or vehicle control. Data are presented as mean ± SEM (n = 10/group).

(C) Aged Vk*MYC mice with an M-spike of at least 15 g/L were treated by intraperitoneal injections for 5 days/week with JQ1 in 10% cyclodextrine (Sigma). SPEP was performed weekly and drug response was calculated by dividing the gamma/albumin ratio at day 0 for each individual M-spike by the gamma/albumin ratio obtained post-treatment. Densitometric profiles obtained at day 0 and day 14 were overlaid to show M-spike reduction with JQ1 treatment.